



HAL
open science

Titan's Interior Structure and Dynamics After the Cassini-Huygens Mission

Christophe Sotin, Klára Kalousová, G. Tobie

► **To cite this version:**

Christophe Sotin, Klára Kalousová, G. Tobie. Titan's Interior Structure and Dynamics After the Cassini-Huygens Mission. *Annual Review of Earth and Planetary Sciences*, 2021, 49 (1), pp.579-607. 10.1146/annurev-earth-072920-052847 . hal-03431284

HAL Id: hal-03431284

<https://hal.science/hal-03431284v1>

Submitted on 5 Jan 2023

HAL is a multi-disciplinary open access archive for the deposit and dissemination of scientific research documents, whether they are published or not. The documents may come from teaching and research institutions in France or abroad, or from public or private research centers.

L'archive ouverte pluridisciplinaire **HAL**, est destinée au dépôt et à la diffusion de documents scientifiques de niveau recherche, publiés ou non, émanant des établissements d'enseignement et de recherche français ou étrangers, des laboratoires publics ou privés.

1 Titan's Interior structure and dynamics after the Cassini/Huygens mission

2 Christophe Sotin¹, Klára Kalousová², and Gabriel Tobie³

3 ¹Jet Propulsion Laboratory-California Institute of Technology, Pasadena, USA

4 ²Charles University, Faculty of Mathematics and Physics, Department of Geophysics, Prague,
5 Czech Republic

6 ³Laboratoire de Planétologie et Géodynamique, UMR-CNRS 6112, Université de Nantes,
7 Nantes, France

8

9 Abstract

10 The Cassini-Huygens mission that explored the Saturn system during the period 2004-2017,
11 revolutionized our understanding of Titan, the only known moon with a dense atmosphere and
12 the only body, besides Earth, with stable surface liquids. Its predominantly nitrogen
13 atmosphere also contains a few percent of methane that is photolyzed on short geological
14 timescales to form ethane and more complex organic molecules. The presence of a significant
15 amount of methane and ⁴⁰Ar, the decay product of ⁴⁰K, argue for exchange processes from
16 the interior to the surface. Here we review the information that constrains Titan's interior
17 structure. Gravity and orbital data suggest that Titan is an ocean world, which implies
18 differentiation into a hydrosphere and a rocky core. The mass and gravity data complemented
19 by equations of state constrain the ocean density and composition as well as the hydrosphere
20 thickness. We present end-member models, review the dynamics of each layer, and discuss
21 the global evolution consistent with the Cassini-Huygens data.

22

23 1. Introduction

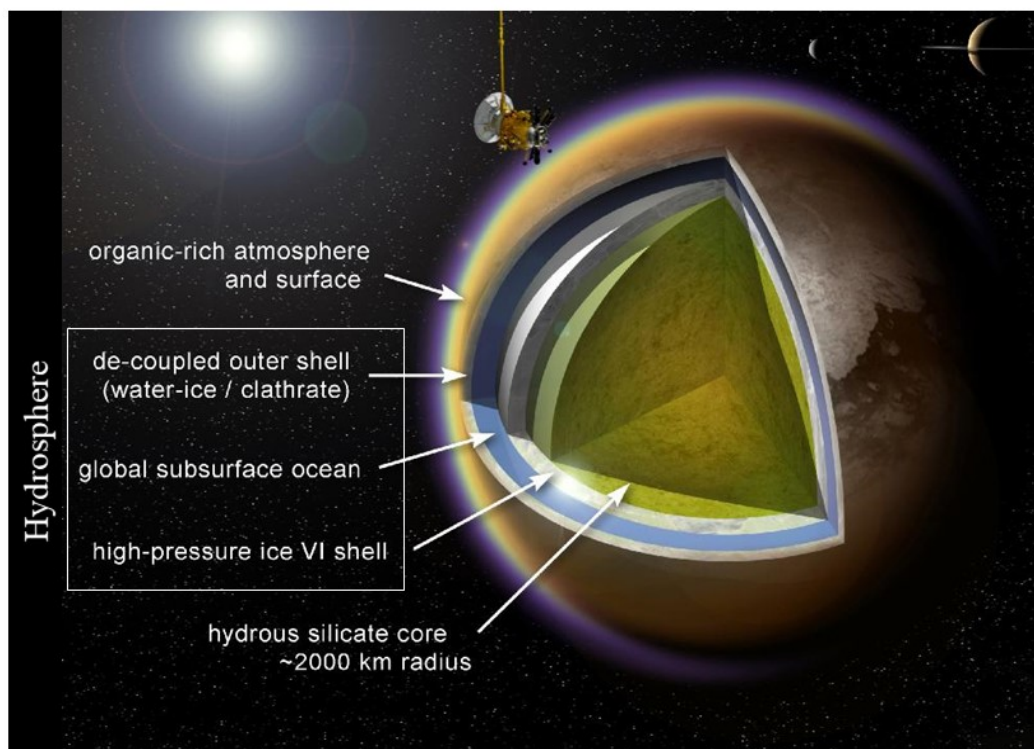
24 Titan is the second largest satellite in the solar system after Jupiter's moon Ganymede. It is
25 the only icy moon with a dense atmosphere made of mostly nitrogen (~98 wt%) and methane
26 (<2 wt%) (Bézard, 2014). The methane abundance varies significantly throughout the
27 atmosphere, from 1.5% in the stratosphere to more than 5% in the troposphere (Niemann et
28 al., 2010; Bézard, 2014). The surface conditions, pressure of 0.15 MPa and temperature of 94
29 K, are such that methane and ethane (produced by photolysis of methane) are liquid and form
30 lakes and seas mostly located at the North pole (Stofan et al., 2007). But methane is
31 irreversibly photolyzed in the upper atmosphere and the present amount would disappear in
32 a few tens of millions of years (e.g. Yung et al., 1984; Griffith et al., 2013), which is short on
33 geological timescales, thus requiring an interior reservoir and a replenishment process. The
34 presence of ⁴⁰Ar, a daughter element from the decay of ⁴⁰K, also implies exchange processes
35 between the K-reservoir, likely silicates, and the atmosphere. Finally, the observed ¹⁵N/¹⁴N
36 isotope ratio suggests that up to 50% of the atmospheric nitrogen could come from the
37 decomposition of insoluble organic matter (IOM) present in Titan's interior (Miller et al., 2019).
38 Understanding the formation of Titan's atmosphere requires knowledge of its interior structure
39 and models of its evolution constrained by observations.

40

41 The NASA-ESA-ASI Cassini-Huygens mission has observed the Saturn system during the
42 period 2004-2017 using Titan's gravity assist to explore the diversity of objects and make in
43 situ measurements at different locations. Determining the interior structure of a planet or
44 satellite from orbit is best achieved by measuring the gravity and magnetic fields. On January
45 14, 2005, the ESA Huygens probe plunged into Titan's atmosphere and provided the first

46 detailed information on Titan's atmosphere (Niemmann et al. 2005, Fulchignoni et al. 2005)
47 and close-up views of Titan's surface (Tomasko et al. 2005). During 13 years, the NASA
48 Cassini spacecraft performed 127 close Titan flybys including nine dedicated to the
49 determination of the gravity field (Iess et al. 2010, 2012; Durante et al., 2019). One important
50 result has been the determination of the tidal Love number k_2 , whose large value implies the
51 presence of a deep ocean (Iess et al., 2012). In addition to being the only moon with a dense
52 atmosphere and the only object in the solar system, besides Earth, with liquids at its surface,
53 Titan is also an ocean world (Fig. 1). The gravity measurements also provided values of the
54 moment of inertia that is an integrated value of the density distribution, suggesting that Titan
55 is differentiated into a hydrosphere and an inner rocky core (Castillo-Rogez & Lunine, 2010).
56 After reviewing the different observations (Section 2), the present paper describes the interior
57 structure models that are consistent with these observations and use the most recent
58 Equations of State (EoS) (Section 3). Section 4 discusses the thermal evolution models and
59 is followed by a discussion of the hydrosphere dynamics and implications for the atmosphere
60 recycling (Section 5).

61



62

63 **Figure 1:** Titan's interior structure adapted from Fortes (2012). The rocky core is likely
64 composed of hydrated silicates to account for the high value of the moment of inertia. It is
65 overlaid by a hydrosphere that includes a deep salty ocean.

66

67 2. Observations

68 Two science questions related to Titan's interior structure that the Cassini-Huygens mission
69 was aimed to answer are: 1) Is there a deep ocean? and 2) How much is Titan differentiated?
70 As proven by previous missions, determining the gravity field, in particular the degree 2
71 coefficients, provides answers to these questions. Additional constraints come from the shape,

72 the electro-magnetic field, the surface morphological features and composition, and the orbital
 73 and rotational characteristics.

74

75 2.1 Gravity coefficients

76 The gravity field provides information on the mass distribution inside Titan. The gravity
 77 coefficients are determined by monitoring the line of sight velocity change of the Cassini
 78 spacecraft as it flies by Titan. The closer to the moon, the more precise the determination of
 79 the gravity field. However, Titan has an extended atmosphere and the drag would add a large
 80 contribution to the spacecraft velocity. An optimum closest approach flyby altitude of 1500 km
 81 was a compromise between the atmospheric perturbations and precision. After the first 4
 82 flybys, less et al. (2010) were able to retrieve the gravity coefficients up to degree 3. The
 83 degree 2 gravity coefficients, J_2 and C_{22} (Table 1) include a constant component and a periodic
 84 component that is proportional to the eccentricity and therefore less than a few percent of the
 85 constant component. Because Titan is in a spin-orbit resonance, it has an ellipsoidal shape
 86 that leads to a high value of the C_{22} coefficient. If Titan is in a hydrostatic equilibrium, the
 87 degree 2 coefficients are related by a simple relation: $J_2 = \frac{10}{3} C_{22}$ The retrieved values (Table
 88 1) give a ratio of 3.19 which is 1.7 standard deviation from the theoretical value of 10/3,
 89 suggesting a slight departure from hydrostatic equilibrium (Durante et al., 2019) (see Section
 90 3.1 for the implication on the interior structure). With the 9 dedicated flybys, Durante et al.
 91 (2019) were able to obtain the gravity field up to degree 5.

92

93 **Table 1:** Parameters for Titan. GM, J_2 , C_{22} , k_2 from Durante et al. (2019), shape parameters
 94 from Corlies et al. (2017), estimated power from Chen et al. (2014). The obliquity value comes
 95 from Stiles et al. (2008).

Semi-major axis to Saturn (km)	1.2218 10 ⁶
Eccentricity	2.846%
Synchronous sidereal rotational period w (s)	1,377,684 ~ 15.945 Earth days
GM (km ³ /s ²)	8978.1383(3)
Mass (10 ²² kg) / density (kg/m ³)	13.4522 (3) / 1881.46 (11)
Mean radius (R) in km	2574.765 (18)
Shape triaxial ellipsoid (a,b,c) in km	2575.124 (26), 2574.746 (45), 2574.414 (28)
Degree 2 gravity coefficients: J_2 and C_{22} (x 10 ⁶)	33.1 (6) 10.38 (8)
Reduced Moment of Inertia (MoI) C/MR ²	0.341
Tidal Love number k_2	0.616 (67)
$q=w^2R^3/GM$	3.96 10 ⁻⁵

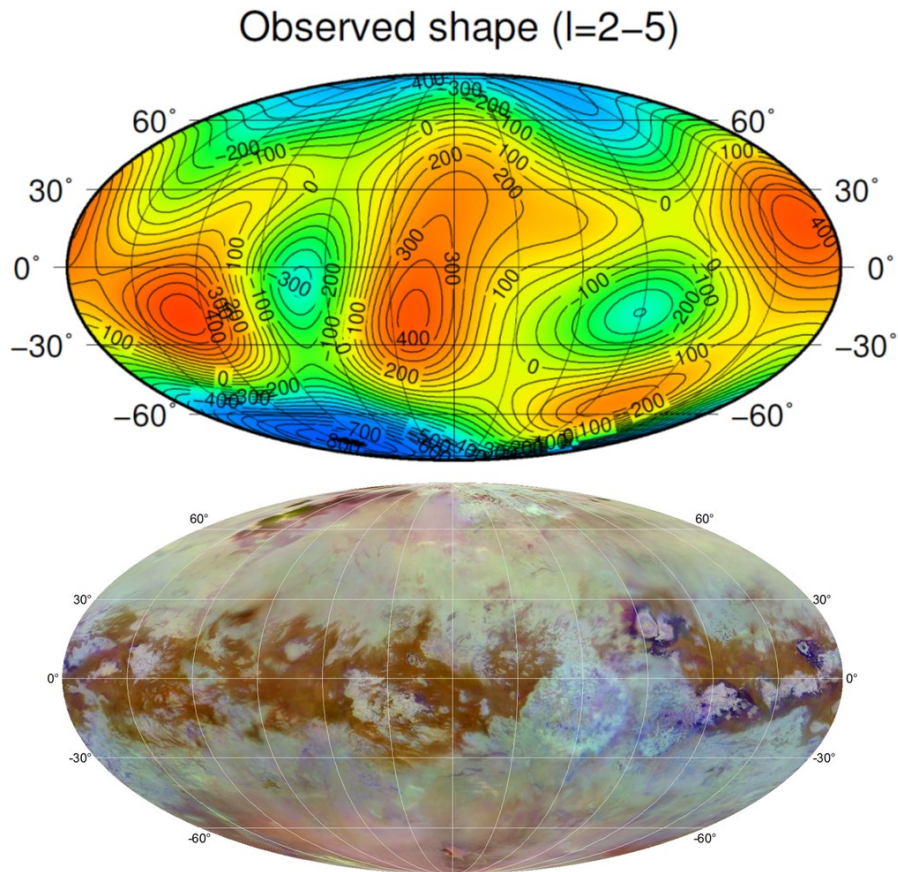
Gravity acceleration (m/s ²) at the surface	1.3543
Estimated radiogenic power (GW)	300 – 400
Obliquity	0.3 deg

96
97
98
99
100
101
102
103
104
105
106
107
108
109
110
111
112
113
114
115
116
117
118
119
120
121
122
123
124
125
126
127
128
129
130
131
132
133
134

It was critical to measure the degree 2 tidal Love number because it puts a strong constraint on the presence of an ocean. This was made possible by having dedicated gravity flybys performed when Titan was near its orbit pericenter and apocenter, maximizing gravity changes (less et al., 2012). The value of k_2 depends on a number of parameters including the ocean density, the ice shell thickness, and the heat transfer mechanism through the ice shell (Mitri et al., 2014). It also depends on the presence of ocean waves that can be triggered if the ocean is stratified. If the ocean is made of pure water, the value of k_2 is around 0.5 (Mitri et al., 2014). Durante et al. (2019) report a value of 0.616, about 1.7 standard deviation larger than the value of 0.5 for pure water. This large value can be explained by either a higher density due to the presence of salts, waves in a stratified ocean, or a combination of the two.

2.2 Shape and topography

Titan's shape was determined by the radar onboard the Cassini spacecraft (Elachi et al., 2004). Three data sets are available (Corlies et al., 2017). First, the Synthetic Aperture Radar (SAR) topography covers ~5.2% of Titan's surface with an average error in elevation of ~160 m over all 122 profiles. Second, the radar in its altimeter mode, mapped ~1.6% of Titan's surface along 69 profiles. Although altimetry provides a much smaller coverage compared to SAR topography, the vertical error is only ~35 m (Zebker et al., 2009). Finally, 19 digital terrain models (DTMs) were constructed through stereophotogrammetry. They cover an additional ~2.1% of Titan's surface, with a typical error of ~100 m (Kirk et al., 2013). These three data sets provide an incomplete coverage of Titan's surface. However, it was possible to retrieve Titan's shape - i.e. the difference between the surface and a sphere of radius 2575 km (Figure 2) - up to a degree 8. The shape is characterized by polar depressions up to 800 m deep. The topography is the difference between Titan's shape and an equipotential surface which is mainly dominated by the first 2 degrees of the gravity field. Titan is characterized by small topography variations at large wavelengths, from about -600 m for the south polar depression to +400 m for some mid-latitude highlands. The polar dynamical flattening can only explain half of the polar depressions observed in the shape model. If these depressions were not isostatically compensated, the J_2/C_{22} ratio would be much larger than the observed value because J_2 strongly depends on uncompensated polar topography (Gao and Stevenson, 2013) whereas C_{22} does not. Therefore, the depressions must be compensated by either a different thickness of the ice shell between the pole and the equator (Airy model proposed by Nimmo and Bills, 2010) or by differences in density (Pratt model proposed by Choukroun and Sotin, 2012). These two models are discussed in Section 5.3 and linked to different physical processes that may operate at Titan - differences in the heat flux transported through the ocean for the Airy model (Section 5.2) and formation of a dense ethane-clathrate layer at the poles for the Pratt model.



135
 136 **Figure 2:** Mollweide projections centered at 180 deg show Titan's shape relative to a 2575 km
 137 sphere (top) and VIMS/ISS color map (bottom) showing the different geological regions (Le
 138 Mouelic et al., 2019). In the upper figure, contours are in m (Corlies et al; 2017 truncated to
 139 degree 5).

140
 141 The depressions at the North pole are consistent with the presence of hydrocarbon seas that
 142 were first observed by the radar instruments (Stofan et al., 2007). A large region named
 143 Xanadu centered at (15 S, 120 W) and extending from 60 W to 150 W also correlates with a
 144 depression (Fig. 2). Other equatorial topographic variations do not seem to correlate with
 145 geological features which are dominated by dune fields (in brown in the VIMS/ISS map, Fig.
 146 2 bottom). As pointed out by Corlies et al. (2017), the absence of dune fields in the Xanadu
 147 region is not explained as the sand would be likely transported to low topography. It suggests
 148 that Xanadu may be a very recent feature.

149
 150 **2.3 Rotational and orbital characteristics**

151 Titan's rotation can provide additional constraints on the internal structure. Neglecting polar
 152 motion, the rotational state of a synchronous satellite can be considered as consisting of two
 153 components: the rotation rate variations with respect to the expected synchronous rotation
 154 rate, i.e. the non-synchronous rotation (NSR) rate, and the obliquity, corresponding to the
 155 angle between the rotation axis and the axis normal to the orbital plane (e.g. Baland et al.,
 156 2014). The value of the NSR rate has been updated several times since its first estimation of
 157 0.36°/year in Lorenz et al. (2008) from radar surface images (see also Stiles et al., 2008).
 158 Lorenz et al. (2008) have interpreted this high NSR rate as evidence of a subsurface ocean,
 159 allowing a decoupling between the deep interior and the ice shell forced by the atmospheric

160 torque. Subsequent data reprocessing by Stiles et al. (2010) indicated a smaller NSR rate
161 (0.11°/year). Using two additional years of data, Meriggiola & less (2012) found a very small
162 NSR rate compatible with synchronous rotation ($\pm 0.02^\circ/\text{year}$). By modeling the gravitational
163 and pressure coupling between the shell and the interior, Van Hoolst et al. (2009, 2013)
164 predicted a maximal NSR rate of about $0.013^\circ/\text{year}$, smaller than the last available estimation
165 of Meriggiola and less (2012), which excludes the possibility to retrieve useful constraints on
166 the interior structure.

167
168 The obliquity of Titan is estimated to be about 0.3° (Stiles et al., 2008; Meriggiola & less,
169 2012), which is about three times larger than 0.12° - the value expected for an entirely solid
170 Titan (Bills & Nimmo, 2008). This high value has been interpreted as being indicative of the
171 presence of an internal ocean (Bills & Nimmo, 2008; 2011; Baland et al., 2011; 2014). By
172 computing the obliquity from a Cassini state model for a differentiated interior structure with
173 each layer having an ellipsoidal shape consistent with the measured surface shape and gravity
174 field, Baland et al. (2014) showed that the observed obliquity implies a relatively dense and
175 deep ocean. However, as a wide range of internal models can explain the observed value, no
176 firm conclusion about the interior structure can be drawn from the obliquity alone.

177
178 Another important constraint on the interior of Titan and its past evolution is provided by the
179 orbital characteristics. Titan exhibits an orbital eccentricity (3%) several times higher than its
180 jovian cousins Europa, Io, and Ganymede. Contrary to the jovian moons, no orbital resonance
181 in the Saturnian system is able to force Titan's eccentricity and thus the frictional damping due
182 to tides raised by Saturn should lead to progressive circularization of Titan's eccentric orbit.
183 The high eccentricity has been classically interpreted as an evidence of reduced dissipation
184 on Titan implying limited surface liquid bodies (Sagan & Dermott, 1982; Sears, 1995) and no
185 liquid water ocean at depth (Sohl et al., 1995). Using a coupled thermal-orbital model, Tobie
186 et al. (2005a, 2006) showed that the current eccentricity may be compatible with the presence
187 of an internal ocean, but would imply a larger eccentricity in the past and an ocean beneath a
188 relatively thin and weakly dissipative ice shell during most of Titan's evolution. The proximity
189 of small Hyperion suggests that the past eccentricity probably never exceeded 0.1-0.2.
190 However, the 4:3 orbital resonance between Hyperion and Titan remains problematic.
191 Recently, using very accurate radio tracking of the Cassini spacecraft during multiple flybys,
192 Lainey et al. (2020) measured Titan's orbital expansion rate. They showed that Titan is
193 migrating outward much faster than initially anticipated, owing to a strong dissipation inside
194 Saturn. This finding implies that Titan formed much closer to Saturn and has migrated outward
195 to its current position. Consequently, Titan experienced much stronger tidal forcing in the past,
196 which may have major implications for its past internal activity.

197 198 **2.4 Atmosphere and surface constraints**

199 The atmosphere composition depends on a number of processes including endogenic
200 processes that lead to outgassing. One major enigma of Titan's global dynamics is the need
201 for methane replenishment against its upper atmosphere photolysis - the present amount of
202 atmospheric methane would be photolyzed in a few tens of million years, which is short on
203 geological timescales (Yung et al., 1984). In the absence of a global surface ocean, the
204 methane reservoir must be in the subsurface where it can be destabilized by internal
205 processes (e.g. Tobie et al., 2006; Choukroun et al., 2010) or by impacts (Choukroun and
206 Sotin, 2012; Zahnle et al. 2014). A large amount of ^{40}Ar (mole fraction of $3.39 (\pm 0.12) \times 10^{-5}$)

207 was measured in Titan's atmosphere by the gas chromatograph mass spectrometer (GCMS)
208 onboard the Huygens probe (Niemann et al., 2010). This corresponds to a total mass of 4.5
209 (± 0.2) 10^{14} kg. Since ^{40}Ar is a product of the radioactive decay of ^{40}K , its presence in the
210 atmosphere indicates its release from the silicates which represent the most likely initial
211 reservoir of ^{40}K . Depending on assumptions on the K/Si ratio in the silicates that composed
212 Titan's rocky core (i.e. the type of chondritic material), the amount of atmospheric ^{40}Ar
213 represents between 10% and 20% of the potential ^{40}Ar . The remaining ^{40}Ar could still be
214 present in the rocky core or dissolved in the ocean or the hydrocarbon seas (e.g. Tobie et al.
215 2012). Finally, a recent study by Miller et al. (2019) suggests that up to 50% of Titan's nitrogen
216 comes from the decomposition of insoluble organic matter (IOM) contained in Titan's rocky
217 core when it warms up. The amount of outgassed nitrogen is inferred from dual considerations
218 of the $^{15}\text{N}/^{14}\text{N}$ isotope ratio (167.7 ± 0.6) and the $^{36}\text{Ar}/\text{N}$ ratio in Titan's atmosphere from
219 Niemann et al. (2010). All the above points demonstrate that exchange processes between
220 the interior and the surface have existed during Titan's geological history although the timings
221 of these outgassing events are not well constrained. Models of Titan's evolution should
222 account for these results.

223

224 Another characteristic of Titan is the paucity of impact craters with only about 60 features that
225 rank from certain (12) to nearly certain (25) to probable (25) (Werynski et al., 2019). The
226 density of impact craters is a proxy for determining the age of a planetary surface. The scarcity
227 of impact craters favors a young age for Titan's surface, between 0.2 and 1 Gyr (Neish &
228 Lorenz, 2012). In addition, the presence of impact craters provides information on the
229 thickness of Titan's lithosphere. The size of Titan's largest impact crater Menrva (diameter of
230 425 km, Figure 2) suggests a lithosphere at least some tens of kilometers thick at the time of
231 formation.

232

233 Finally, the surface composition can provide information about a potential resurfacing. Titan's
234 surface is covered with organic aerosol forming in its upper atmosphere by the photolysis of
235 methane and further reactions with nitrogen (e.g. Hörst, 2017). All of Titan's surface should be
236 coated with these aerosols that eventually turn into sand to form the dune fields. However,
237 some areas appear different in false-color infrared images of Titan's surface (Fig. 2, bottom) -
238 the dark blue color is interpreted as regions enriched in water ice (Griffith et al., 2019; Le
239 Mouelic et al., 2019). The origin of these terrains seems to be related to exogenic processes
240 such as impact craters (e.g. Le Mouelic et al., 2008) and erosion (Jaumann et al., 2008; Griffith
241 et al., 2019). Evidence for endogenic processes is limited to a potential cryovolcano in the
242 Sotra Facula regio (Lopes et al., 2013) and tentative interpretation of flow-like features in Tui
243 and Hotei regio (Barnes et al., 2006). Confirmation that these features have a volcanic origin
244 would require higher resolution observations as well as composition information.

245

246 **2.5 Electro-magnetic measurements**

247 Magnetic field measurements can provide key information on the interior structure of an ocean
248 world as demonstrated by the Galileo mission. The magnetometers on the Galileo spacecraft
249 detected Ganymede's permanent magnetic field best interpreted by the presence of an iron-
250 rich liquid core (Kivelson et al., 1996). They also detected inductive magnetic fields at
251 Ganymede, Europa and Callisto (Kivelson et al., 2002; Khurana et al., 1998) which are best
252 interpreted by the presence of a deep salty ocean. However such measurements at Titan are
253 challenged by three facts (e.g. Saur et al. 2010). First, the presence of the dense atmosphere
254 prevents any flyby closer than 1000 km. Second, the almost perfect alignment of Saturn's

255 magnetic dipole axis with its spin axis prevents large variations of Saturn's magnetic field along
256 Titan's orbit. Third, Titan's ionosphere adds a large external component that must be removed
257 before retrieving the internal component. The Cassini magnetometer team has not reported
258 any evidence of a permanent magnetic field or an inductive one.

259

260 During its descent through Titan's atmosphere in January 2005, the Huygens probe measured
261 the horizontal and vertical components of the electric field with the Permittivity, Wave and
262 Altimetry (PWA) instrument (Béghin et al., 2007). A few Hz wide signal centered at 36 Hz is
263 present almost continuously throughout the descent. A careful analysis of the data (Simoes et
264 al., 2007) suggested that this signal is of natural origin and would have been the second
265 eigenmode of a Schumann-like resonance in Titan's atmospheric cavity. The Schumann
266 resonance on Earth is the propagation of an electric signal within a cavity limited by two
267 conductive layers which are the ionosphere on the top and the surface (mainly the ocean) at
268 the bottom. The frequency of the resonance is linked to the size of the cavity. On Earth, the
269 Schumann resonance is triggered by powerful atmospheric lightning activity. To date, such a
270 source has not been detected on Titan (Fischer & Gurnett, 2011). Another process that could
271 trigger the propagation of the waves is a plasma instability mechanism associated with the
272 corotating Saturnian plasma flow (Béghin et al., 2007, 2012). However, a recent analysis of
273 the signal recorded by the PWA instrument demonstrates a very strong correlation with the
274 history of mechanical vibrations such as parachute release (Lorenz & Le Gall, 2020). It seems
275 likely that the PWA signal is due to vibrations of the boom in the electric field present in Titan's
276 atmosphere and cannot be used to infer the depth of an electrically conductive ocean.

277

278 During the course of the Cassini-Huygens mission, four independent observations were
279 discussed as evidence for the presence of a deep ocean: obliquity, degree 2 tidal Love
280 number, nonsynchronous rotation, and Schumann resonance. Only two of them survived a
281 more thorough analysis: obliquity and degree 2 tidal Love number. The degree 2 gravity
282 coefficients suggest that Titan is differentiated although not as much as Ganymede, which is
283 consistent with the lack of a permanent magnetic field generated in an iron-rich liquid core.
284 Titan thus consists of a silicate core overlaid by a hydrosphere that includes a deep ocean
285 (Fig. 1). The next section describes interior structure models that are consistent with EoS for
286 aqueous solutions and silicates.

287

288 **3. Interior structure**

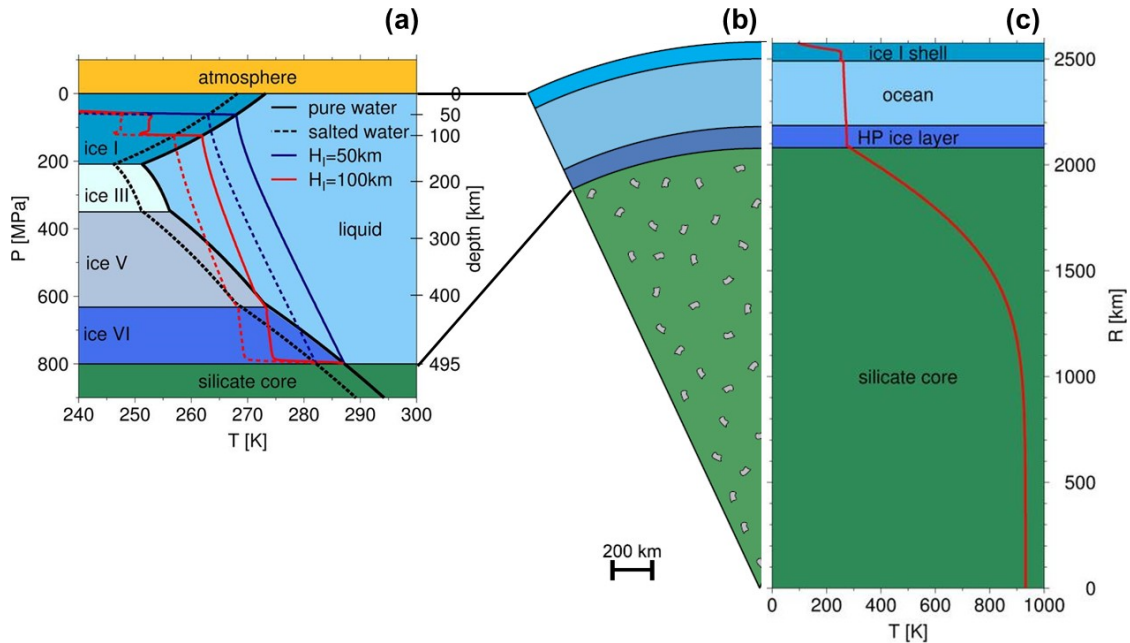
289 **3.1 Modeling the interior structure**

290 Any model of Titan's interior must satisfy the observational constraints presented in Section
291 2. Its average density of 1881 kg.m^{-3} suggests a large fraction of water ice and other low-
292 density compounds. The interior structure of Titan may consist of up to 5 main layers (from
293 center to surface): a rocky core, a high-pressure (HP) ice VI-V layer, a liquid water ocean, an
294 ice I shell and possibly a chemically distinct icy crust enriched in hydrocarbon elements
295 (Figure 3). The radius and density of these different layers is determined in order to satisfy the
296 average surface radius, total mass and the moment of inertia (Mol) factor (Table 1). Even if
297 those quantities are well constrained, there are no unique solutions of the problem - different
298 combinations of layer densities and thicknesses can reproduce the observed global values.

299

300 In each layer, the mass, gravity, pressure and Mol are integrated from the material density
301 which is determined by a given composition/phase using the appropriate Equation of State
302 (EoS, see Section 3.2). The density variations with depth are determined from the pressure

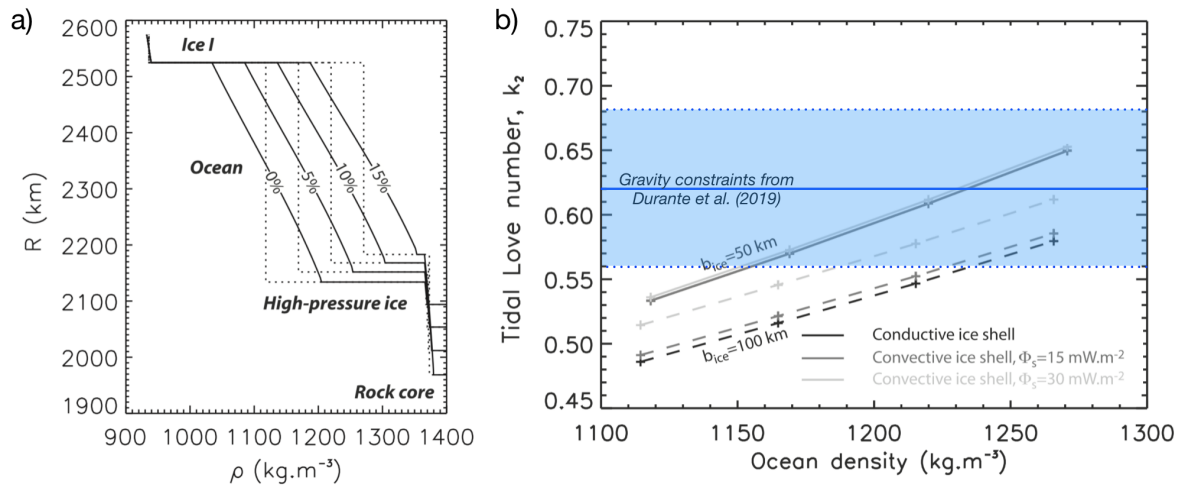
303 and the temperature, which requires the construction of a temperature profile in each layer.
 304 The position of the top and bottom ocean interfaces is determined by the intersection of the
 305 water ice melting curve and the temperature profile in the ocean (see Figure 3a). Both the
 306 melting curve and the ocean adiabat depend on the ocean composition (e.g. Vance et al.,
 307 2018).
 308



309 **Figure 3:** (a) Pressure-temperature diagram for conditions in Titan's hydrosphere. Black lines
 310 indicate the melting curve for pure H₂O (full lines, Wagner et al., 1994, 2011) and salty
 311 hydrosphere (dashed lines, 5K colder). Blue and red profiles correspond to ice I shell thickness
 312 $H_i =$ of 50 and 100km, respectively. The depth on the right vertical axis is approximate and
 313 corresponds to pure hydrosphere. Adapted from Kalousová & Sotin (2020a). (b) Interior
 314 structure of Titan from Néri et al. (2020) where the orange symbols indicate the presence of
 315 insoluble organic matter (IOM). (c) A possible temperature profile in Titan (see text for details).
 316
 317

318 Due to the physics of the crystallization processes, the outer ice shell and the high-pressure
 319 ice layer are believed to be composed of almost pure water ice, for which the density is well
 320 known in the pressure range expected in Titan's interior (e.g. Choukroun & Grasset, 2010).
 321 The main uncertainties are the thickness of the outer ice shell, the density (composition) of
 322 the ocean and the density of the rocky core which can vary significantly depending on the
 323 assumed composition. The ocean composition also affects the melting curves. Owing to its
 324 strong depression of the crystallization temperature, ammonia has been commonly
 325 considered when modeling the evolution of Titan's hydrosphere (Lunine & Stevenson, 1987;
 326 Grasset & Sotin, 1996; Tobie et al., 2005a). These models showed that the presence of a few
 327 percent of ammonia would help the preservation of a subsurface ocean inside Titan. A few
 328 percent of ammonia, however, reduces the density of the aqueous solution compared to pure
 329 water (Croft et al., 1988). This appears incompatible with the estimate of the tidal Love number
 330 (less et al., 2012; Durante et al., 2019), which points to an ocean denser than pure water.
 331 According to the analysis of Mitri et al. (2014) (Figure 4b), the average ocean density should
 332 be at least 1150 kg.m^{-3} if the ice shell is 50 km thick, and at least 1190 kg.m^{-3} for a 100 km
 333 thick convective ice shell. This implies that the ocean should contain a non-water component
 334 that increases the density by about 5-10% relative to pure water (Figure 4a). Various
 335 compounds have been proposed such as ammonium sulfate (Fortes et al., 2007), sodium

336 chloride or magnesium sulfate (Vance et al., 2018). Based on the existing data, it is impossible
 337 to determine which one is more likely.
 338



339 **Figure 4:** (a) Density profiles in the hydrosphere for different oceanic compositions. (b)
 340 Predicted tidal Love number as a function of average ocean density for two different ice shell
 341 thicknesses (50 and 100 km) in a conductive or convective state. Adapted from Mitri et al.
 342 (2014).
 343
 344

345 By constraining the hydrosphere structure from the tidal Love number estimate and the phase
 346 diagram consideration, it is then possible to determine the size and density of the rocky core
 347 from the moment of inertia as explained in Vance et al. (2014) for Ganymede. The Mol factor
 348 (C/MR^2) is inferred from the degree 2 gravity coefficients, J_2 and C_{22} , using the Radau-Darwin
 349 approximation which assumes that the gravity field is mostly determined by the dynamical
 350 distortion of a radially-distributed density structure in response to rotational and tidal forces.
 351 The fact that the J_2/C_{22} ratio is not exactly equal to 10/3 (Durante et al., 2019) and the existence
 352 of non-negligible higher degrees gravity coefficients indicate a departure from the ideal
 353 hydrostatic response. As noted in Section 2.2, the topography variations do not correlate with
 354 the higher degree gravity coefficients. A global inversion of gravity and topography is required
 355 in order to determine the magnitude of the non-hydrostaticity, which would lead to a slightly
 356 smaller value of the Mol. The lower the Mol, the larger the differentiation. It seems however
 357 very unlikely that the Mol would be as low as for Ganymede (0.311) where an iron-rich liquid
 358 core is present.
 359

360 Even small variations in the value of the Mol factor can have major implications for the
 361 composition of the rocky core. A value of 0.34 implies a rocky core density of the order of
 362 2550-2650 $\text{kg}\cdot\text{m}^{-3}$ for a core radius ranging between 2100 and 1970 km, whereas the density
 363 would range between 2850 and 3100 $\text{kg}\cdot\text{m}^{-3}$ and the radius from 1950 to 1770 km for a value
 364 of 0.33 (Mitri et al., 2014; Néri et al., 2020). The variability in core density and radius for a
 365 given value of the Mol is mostly controlled by the ocean density and the outer ice shell
 366 thickness (Mitri et al., 2014). As discussed in Section 3.2, these values of density are smaller
 367 than values inferred from the EoS of silicates and iron phases that form carbonaceous
 368 chondrites which are assumed to be one of the building blocks of silicate rich bodies in the
 369 outer solar system. The low density of the core implies either an incomplete differentiation, or
 370 a content in iron that would be much less than in carbonaceous chondrites, or the existence
 371 of a low density compound mixed with the rock phase. O'Rourke & Stevenson (2014)

372 performed numerical simulations of double diffusive convection to assess whether Titan could
373 be partially differentiated, i.e. have a mixture of ice and rock in its core. Their study shows that
374 although the differentiation could be delayed, present Titan is not partially differentiated even
375 if ^{40}K , a major component of the radioactive heating, was leached from the core. Similarly,
376 there is no observation or theory that would support an iron content in the building rocks of the
377 Saturnian moons being smaller than in chondrites. The same is true for the Jovian system. If
378 iron concentration is left as a free parameter, it leads to Fe/Si ratios much lower than the
379 chondritic value but no formation model accounts for large variations of the Fe/Si ratio inferred
380 in Jovian satellites (Sohl et al., 2002). A remaining possibility is a low density compound of the
381 rocky core for which Néri et al. (2020) proposed that it may be the insoluble organic matter
382 (IOM) whose mass fraction could range between 15 and 25 wt% for Mol factor between 0.33
383 and 0.34 (Figure 3b). This proposition is consistent with the finding of Miller et al. (2019) that
384 up to 50% of Titan's atmospheric nitrogen comes from the decomposition of IOM. The
385 presence of IOM in Titan's core would have major consequences for the differentiation and
386 evolution of Titan's interior.

387

388 **3.2 Equations of State of water and silicates**

389 Determining the internal structure of Titan compatible with the existing observational
390 constraints requires the use of appropriate EoS for water compounds and silicate minerals.
391 For the pressure and temperature ranges expected in Titan's hydrosphere (100-350 K, 1.5 bar
392 - 1 GPa), several ice polymorphs, aqueous solutions of varying compositions, gas hydrates
393 and hydrated salts are predicted. Following the pioneer work of Lunine & Stevenson (1987),
394 most of the internal models considered ammonia-water solutions and $\text{NH}_3\text{-H}_2\text{O}$ phase diagram
395 as representative materials for Titan's hydrosphere. Consequently, the experimental works
396 have been focused on the acquisition of thermodynamic data for the $\text{NH}_3\text{-H}_2\text{O}$ system (Croft
397 et al., 1988; Grasset & Sotin, 1996; Hogenboom et al., 1997; Grasset & Pargamin, 2005;
398 Choukroun & Grasset, 2010). The density constraint provided by Titan's tidal Love number
399 ruled out ammonia as a main constituent of Titan's ocean and suggests rather heavier ionic
400 species such as NaCl , MgCl_2 , MgSO_4 , Na_2SO_4 , $\text{NH}_4(\text{SO}_4)_2$, etc.

401

402 Quantifying the effect of these ionic species on the thermodynamic properties of aqueous
403 solutions and on the phase diagram of salt-water system is essential to correctly predict the
404 structure and thermal state of the hydrosphere. The Na-Mg-Cl- SO_4 -water systems have been
405 extensively studied below 100 MPa (Journaux et al., 2020a), but, with the exception of
406 MgSO_4 -water system (Vance & Brown, 2013), they remain poorly known at higher pressure
407 that is relevant for Titan's hydrosphere. Sound speed measurements at high pressure
408 (Bollengier et al., 2019) are currently under finalization in order to constrain these different
409 salt-water systems. Following the approach developed for pure water system (Brown, 2018;
410 Bollengier et al., 2019), it is possible to derive a Gibbs energy representation of these systems
411 that allows the derivation of the different thermodynamic quantities (density, thermal
412 expansion, heat capacity, chemical potential) relevant for modeling the adiabatic profile
413 through the ocean and the water/ice phase boundaries. First application using this
414 representation has already been applied to the MgSO_4 -water system (Vance et al., 2018) and
415 should be generalized in the future to other systems using the SeaFreeze software developed
416 for that purpose (Journaux et al., 2020b).

417

418 The density profile in the rocky core can be calculated by using an elementary composition
419 that is consistent with cosmochemical models (Mueller & McKinnon, 1988). Alternatively, Néri

420 et al. (2020) took the elementary composition of carbonaceous chondrites from Wasson &
 421 Kallemeyn (1988). The density of the silicates is computed using the thermodynamic software
 422 Perple_X (Connolly, 1990) along a pressure-temperature profile consistent with the
 423 conductive heat transfer in a rocky core heated by the decay of the long-lived radioactive
 424 elements (Castillo-Rogez & Lunine, 2010, Figure 3c). The density of other components (iron
 425 sulfide and IOM) is determined from laboratory measurements.

426
 427 **Table 2:** Characteristics of 2 possible models of Titan's interior structure. Model 1 is a nominal
 428 pure H₂O model with a thick convective ice shell whereas Model 2 has a salty ocean (denser)
 429 with a thinner conductive crust.

		Model 1	Model 2
		convection in the outer ice shell - MoI of 0.341	conduction in the outer ice shell - MoI of 0.330
Ocean depth	km	112	36
Ocean density	kg/m ³	1.122	1.219
Ocean thickness	km	250	502
HP ice thickness	km	130	180
Ocean mass	10 ²² kg	1.92	4.04
Rocky core radius	Km	2083	1856
Rocky core density	kg/m ³	2565	2975
Hydrosphere mass	10 ²² kg	3.74	5.48
Rocky core mass	10 ²² kg	9.71	7.97

430
 431
 432 **3.3 Comparison between different interior structure models**
 433 Although the measurements from the Cassini-Huygens mission coupled with the recent
 434 laboratory data on the EoS of the different components provide new constraints on Titan's
 435 interior structure, there are still a lot of unknowns such as the thickness of the outer ice shell,
 436 the presence and distribution of clathrates therein, the thickness, density and composition of
 437 the ocean, the thickness of the high-pressure (HP) ice layer, and the composition of the rocky
 438 core. Figure 3a (full red line) shows a nominal model for a pure H₂O ocean and a ~100 km
 439 thick ice shell (Kalousová & Sotin, 2020a). Using the H₂O EoS of the different phases, one
 440 can compute the thickness of the ocean, the thickness of the HP ice layer, and the radius and
 441 density of the rocky core. The very low density of the silicate core (2565 kg m⁻³, Table 2)
 442 compared to that of carbonaceous chondrites at the relevant (P,T) conditions (Figure 3c)
 443 requires the addition of about 25% IOM. In this model, the temperature profile remains below
 444 the dehydration temperature of the silicates (Fig. 3c), which suggests that a large fraction of
 445 potassium was leached during differentiation. Model 2 has a thinner conductive ice shell, a

446 denser (salty) ocean, and a smaller value of the Mol to account for some potential non-
447 hydrostatic effects (e.g. Durante et al., 2019). This model is also consistent with a value of
448 0.62 for the tidal Love number (Table 2 and Fig. 4). As a result, the radius of the rocky core is
449 smaller, its density larger but still lower than that of carbonaceous chondrites at these (P,T)
450 conditions, and the thickness of the HP ice layer is larger. If the salt is sodium chloride that
451 was leached from the rock fraction during differentiation, the amount of Chlorine required to
452 get a density of 1.219 is about 50 times as large as the amount available in the silicates
453 assuming a carbonaceous chondrite Cl/Si ration (Wasson and Kallemeyn, 1988). However,
454 the space of possible models is quite large. Further studies are required to investigate the
455 most likely interior model that can satisfy all the information available for Titan.

456

457

458 **4. Internal differentiation and evolution**

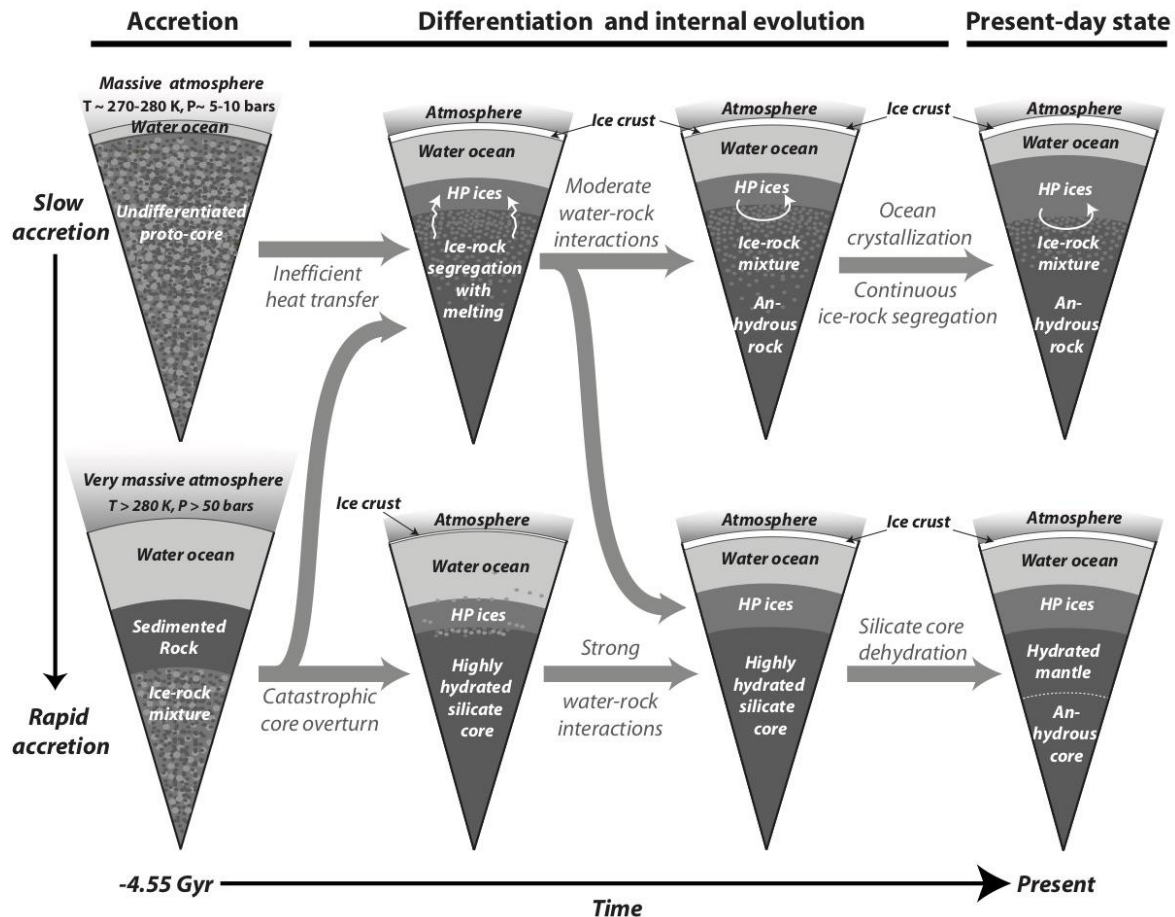
459 **4.1 Accretion and formation of a primitive ocean and atmosphere**

460 During the very early stage of Titan's evolution, the accretional (impact) heating is the
461 predominant heat source and determines the initial structure and post-accretional thermal
462 state of Titan's interior (Figure 5). The impact heating results from the deposition of impactor
463 kinetic energy during the satellite accretion and it thus depends on the impactor velocity as
464 well as on the fraction of kinetic energy that is converted into heat. The impact creates a shock
465 wave that compresses the satellite - below the impact site, the peak pressure is almost uniform
466 in a quasi-spherical region called the isobaric core (e.g. Croft, 1982; Senshu et al., 2002).
467 Energy balance between the impactor kinetic energy and the impact heating leads to a local
468 temperature increase proportional to the square of the growing icy moon radius (e.g. Monteux et
469 al., 2007). As long as the growing moon radius is below 1000 km, the local temperature
470 increase is less than 10-15 K after each impact. Above 2000 km, the increase of temperature
471 is larger than 50 K. During accretion, the global increase of surface temperature depends on
472 how deep the energy is buried, which is controlled by the impactor size, and how frequently
473 the successive impacts occurred.

474

475 By modeling the satellite accretion in 3D from a swarm of impactors of various sizes, Monteux
476 et al. (2014) tested the influence of impactor size distribution on the thermal evolution of a
477 growing satellite. They showed that for satellites exceeding 1500-2000 km, surface melting
478 can be avoided only if the satellite accreted relatively slowly (>1 Myr) from small impactors (<1
479 km) and if the conversion of impact energy into heat is unrealistically inefficient (<10-15%),
480 confirming the earlier estimations of Barr et al. (2010). However, as soon as a small fraction
481 (>10%) of the impactors exceeds 1km, global melting of the outer layer of the growing satellite
482 cannot be avoided. As a result, a ~~the~~ surface ocean forms that is in equilibrium with a massive
483 primitive atmosphere generated by the release of volatiles brought by the icy impactors
484 (Kuramoto & Matsui, 1994; Marounina et al., 2018).

485



486
 487 **Figure 5:** Possible evolution scenarios for the interior of Titan for different initial states.
 488 Depending mostly on the efficiency of heat transfer in the interior, different bifurcations in the
 489 evolutionary path may have occurred. Adapted from Tobie et al. (2014).

490
 491 The volume of the surface ocean depends on the efficiency of accretion processes. For a slow
 492 accretion with small impactors, melting occurred at the end of accretion, resulting in the
 493 formation of a few tens of kilometers thick ocean and an atmosphere of <10 bars. On the other
 494 hand, for rapid accretion with large impactors, melting could occur when the satellite radius
 495 reached 1000 km (about 40% of its final radius and less than 10% of its final mass), leading
 496 to the formation of a very thick water layer in equilibrium with an atmosphere with the surface
 497 pressure exceeding 50 bar (Tobie et al., 2012; 2014). Marounina et al. (2018) showed that the
 498 atmosphere originating from the devolatilization of icy impactors was mostly composed of CO₂
 499 and CH₄, which contrasts with the present N₂-dominated atmosphere. Melting of infalling icy
 500 impactors also released rock particles that sedimented at the base of the ocean. During this
 501 post-accretional period, the pressure at the base of the ocean was not large enough to lead
 502 to the formation of a high-pressure layer and the water ocean directly interacted with the
 503 sedimented rock layer, potentially promoting large-scale water-rock interactions and
 504 production of CH₄ and other gas compounds (Glein, 2015).

505
 506 **4.2 Heat budget and water-ice-rock segregation**
 507 Saturn likely formed after Jupiter (e.g. Sasaki et al., 2010) so when Titan formed, most of the
 508 short-lived radioactive isotopes (mainly ²⁶Al) were already decayed and did not contribute
 509 significantly to the early internal heat budget. The main heat source was provided by the decay

510 of long-lived radiogenic elements, mostly ^{40}K and ^{235}U , during the first billion of years. To
511 estimate the heat power generated by the radiogenic decay of the rock phase in the moons,
512 chondrites can be used. For Titan, carbonaceous chondrites, which are believed to be the
513 dominant types of chondrites beyond Jupiter (Kruijjer et al., 2017), are commonly assumed as
514 a good proxy of the rock phase (Fortes, 2012; Tobie et al., 2012; Glein, 2015; Néri et al.,
515 2020). Assuming a composition dominated by CI chondrites, the total radiogenic power just
516 after accretion is estimated to be about 2.5 TW and progressively decay with time to ~300 GW
517 at present (Husmann et al., 2010).

518
519 Heat generated by tidal friction inside Titan due to the gravitational interaction with Saturn may
520 have also significantly varied during Titan's history. Contrary to the Jupiter system where the
521 Laplace resonance forces the moons' eccentricity, the absence of strong orbital resonance
522 forcing Titan's eccentricity suggests that the eccentricity of Titan, which is already large (~3%),
523 was even larger in the past, potentially resulting in tidal heating comparable to Europa's (Tobie
524 et al., 2005b). The recent analysis of Lainey et al. (2020) further indicates that Titan may have
525 formed much closer to Saturn and migrated outward due to resonance locking with Saturn. At
526 present, the global dissipation in Titan is estimated to be <200 GW (Tobie et al., 2005b;
527 Kalousová & Sotin, 2020b), but it may have been much larger in the past, potentially exceeding
528 several TWs. During the very early stage, Titan also experienced strong tidal despinning
529 before reaching the tidally-locked spin-orbit resonance. Although the associated dissipation
530 rate is very large, it lasted for short periods of time, on the order of 100,000 years (Husmann
531 et al., 2010), resulting in a moderate increase of internal temperature of 25-50 K (Tobie et al.,
532 2014).

533
534 A third source of energy resulted from the release of gravitational energy associated with the
535 internal differentiation (Friedson & Stevenson, 1983; Husmann et al., 2010). An
536 approximative estimate of the temperature increase due viscous heating associated to ice-
537 rock separation can be obtained by considering the difference of gravitational energy between
538 an initially homogeneous interior and a differentiated interior with a full separation of rock and
539 ice phases. This corresponds to a maximum temperature increase of the order of 100-150 K
540 (Tobie et al., 2014). This does not include the heat loss associated to convective transfer,
541 which is particularly important if a large fraction of the interior is molten, as discussed in section
542 4.1. The total heat budget, including radiogenic heating, tidal viscoelastic heating and viscous
543 heating, determines the timing of the differentiation process. Enhanced tidal dissipation may
544 for instance trigger earlier differentiation process, and was suggested to explain the difference
545 in differentiation state between Callisto and Ganymede (Showman & Malhotra, 1999).

546
547 If the ice-rock separation is fast enough (<0.5 Gyr), the dissipation of potential energy may
548 induce runaway melting and thus lead to a catastrophic differentiation, as proposed for
549 Ganymede (Friedson & Stevenson, 1983; Kirk & Stevenson, 1987). This corresponds to the
550 scenario shown on Figure 5 (second row). If the differentiation process is slower and more
551 gradual (>1 Gyr), the convective heat transfer should be able to transport the additional energy
552 and prevent internal melting, as proposed for Callisto (Nagel et al., 2004). More recently,
553 O'Rourke & Stevenson (2014) showed that double-diffusive convection in a mixed ice-rock
554 interior can delay internal melting and ice-rock separation, but cannot prevent it, even if
555 reduced radiogenic power is assumed (see Figure 5, first row). This indicates that it is difficult
556 to prevent full separation between the rock and the hydrosphere. We should keep in mind,
557 however, that the duration of the differentiation process depends on the rheology of ice-rock

558 mixtures, which is poorly constrained at high pressures. Further experimental and modeling
559 efforts are required to better understand the differentiation processes of large icy moons.

560

561 **4.3 Water-rock interactions and conditions for the (non)formation of an iron- core**

562 After the separation of rock and ice, water-rock interactions are limited to the ice-rock interface
563 at the base of the high-pressure layer. Even though water at this interface is mostly in the form
564 of a high-pressure ice phase owing to the elevated pressure (>0.8 – 1 GPa), liquid water may
565 locally exist and potentially circulate through the upper part of the rocky core. Depending on
566 the efficiency of heat transfer through the high-pressure ice layer which is mostly controlled
567 by the poorly-known viscosity of HP ice (Kalousová et al., 2018, see also Section 5), the
568 formation of transiently present liquids at the rock-ice interface may be possible (Kalousová &
569 Sotin, 2020a). These liquids could interact with the underlying rocks before percolating
570 upward to the ocean. Warm liquid water may be also released from the core when the
571 dehydration temperature is reached (Castillo-Rogez & Lunine, 2010). This dehydration event
572 may have occurred relatively late during Titan's evolution (>3 – 3.5 Gyr after formation),
573 provided that sufficient amounts of radiogenic potassium were leached from the core and that
574 thermal diffusivity in the core is not too low (Castillo-Rogez & Lunine, 2010). In the warm
575 evolution scenarios, intensive water-rock interactions were likely during two main sequences
576 of Titan's evolution - before 1 Gyr during the differentiation and after 3-3.5 Gyr during the core
577 dehydration.

578

579 Dehydration processes may not occur if the hydrated silicate core can convect, thus removing
580 the radioactive heat efficiently. Hydrated silicates have a deformation rate that strongly
581 depends on stress and only weakly on temperature (Hilairt et al., 2007). To date, no study
582 has investigated the possibility of convection in the hydrated silicates. If convection does not
583 start in the hydrated silicates, then dehydration may start in the center of the moon (Castillo-
584 Rogez and Lunine, 2010). The dehydration temperature is 350 K lower than the eutectic
585 temperature of the Fe-FeS system (1200 K at Titan's interior pressure, Buono et al., 2011). If
586 the amount of internal heating is large enough, then the temperature may exceed the Fe-FeS
587 system eutectic temperature and an iron core may form, a process that may have happened
588 on Ganymede (Bonnet-Gibet et al., 2020). The lack of intrinsic magnetic field at Titan may
589 indicate that such high temperatures may not have been reached inside Titan.

590

591 **5. Dynamics and evolution of the hydrosphere**

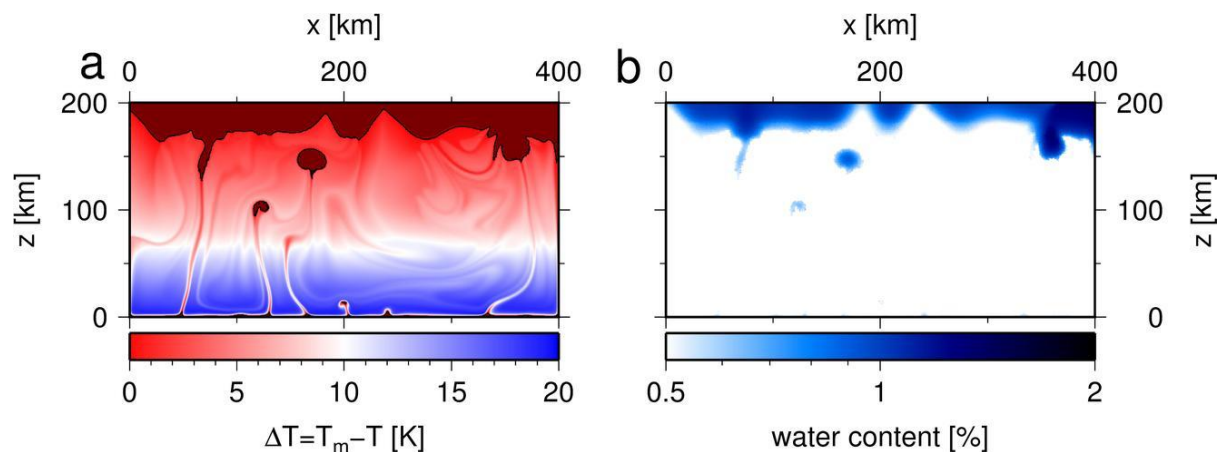
592 Based on the interior structure models, Titan's hydrosphere is about 500 km thick (see Section
593 3). It harbors a subsurface water ocean which is sandwiched between the outer ice shell and
594 a deep ice layer possibly composed of several high-pressure (HP) ice phases (ice VI, V, and
595 III, see Fig. 3). We first review recent models describing the dynamics and heat transfer in the
596 particular hydrosphere layers before addressing the coupled evolution of the hydrosphere as
597 a whole.

598

599 **5.1 Dynamics of the HP ice layer**

600 Titan's HP ice layer is supplied with radiogenic heat flow from the underlying silicate core
601 (Section 4) and its top boundary is determined by the intersection of the ocean adiabat and
602 the melting curve (Section 3). Its dynamics is mainly controlled by the HP ices viscosity which
603 has been measured by several groups (Sotin et al. 1985; Sotin and Poirier, 1987; Durham et
604 al. 1996; 1997; see also Journaux et al., 2020a, for a compilation). The temperature difference
605 between the bottom and top boundary is less than ~ 30 K (Fig. 3) and thus the ice temperature
606 is always close to the melting curve. This has two implications. First, the viscosity is low
607 enough for thermal convection to occur (Choblet et al., 2017a; Kalousová & Sotin, 2020a).
608 Second, the melting temperature is reached for a broad range of models (Choblet et al.,
609 2017a) and thus a two-phase mixture model is necessary to self consistently treat the melting
610 process and the subsequent melt evolution. Figure 6 shows a snapshot from a two-phase
611 convection simulation tailored to Titan's HP ice layer from Kalousová & Sotin (2020a). The left
612 panel depicts the temperature difference from the melting temperature (note that $\Delta T \leq 20$ K)
613 with the dark red denoting the partially molten (temperate) ice where temperature equals the
614 melting temperature ($T=T_m$) and where some water may be present. The right panel shows
615 the corresponding water content (porosity Φ) - note that only a few percent are present and
616 no melt accumulation is observed. Due to the decrease of the melting temperature with the
617 decreasing pressure (i.e. increasing vertical coordinate, see Fig. 3), most of the water is
618 produced in the top layer of temperate ice at the ocean interface from where it is extracted into
619 the ocean. Due to this temperate layer, no cold thermal boundary layer (TBL) is present and
620 the convection is thus characterized by the hot upwelling plumes generated in the hot TBL
621 and a passive downwelling. Some water may be also present in the upwelling plumes and at
622 the silicates interface. Scaling performed by Kalousová & Sotin (2020a) showed that the
623 occurrence or not of bottom melting mainly depends on the incoming heat flux, the ice viscosity
624 and the HP ice layer thickness. For the currently expected interior structure (Section 3), the
625 amount of heat produced in the core (Section 4) and reasonable viscosity values, Kalousová
626 & Sotin (2020a) predict that melt may be present at the interface of Titan's core and HP ice
627 layer. This has profound astrobiology implications since volatiles and organics present in
628 Titan's core may be leached and transported by the liquids into the ocean (Section 4). This
629 makes Titan quite different from Ganymede whose HP ice layer is probably much thicker and
630 melt is not currently predicted at its bottom (Kalousová et al., 2018; Kalousová & Sotin, 2018).
631 Let us note that all the described models were performed assuming a pure H_2O setting. If
632 other compounds such as ammonium sulfate, magnesium sulfate, or sodium chloride are
633 present in the ocean (Section 3), the processes described above may be altered since the
634 melting temperatures as well as the liquid densities would be changed substantially.

635



636
637

638 **Figure 6:** Heat and water transport through Titan's HP ice layer. (a) Temperature difference
639 from the melting temperature ($\Delta T = T_m - T$). Dark red marks the temperate ice ($T = T_m$). (b)
640 Water content (porosity). Adapted from Kalousová & Sotin (2020a).
641

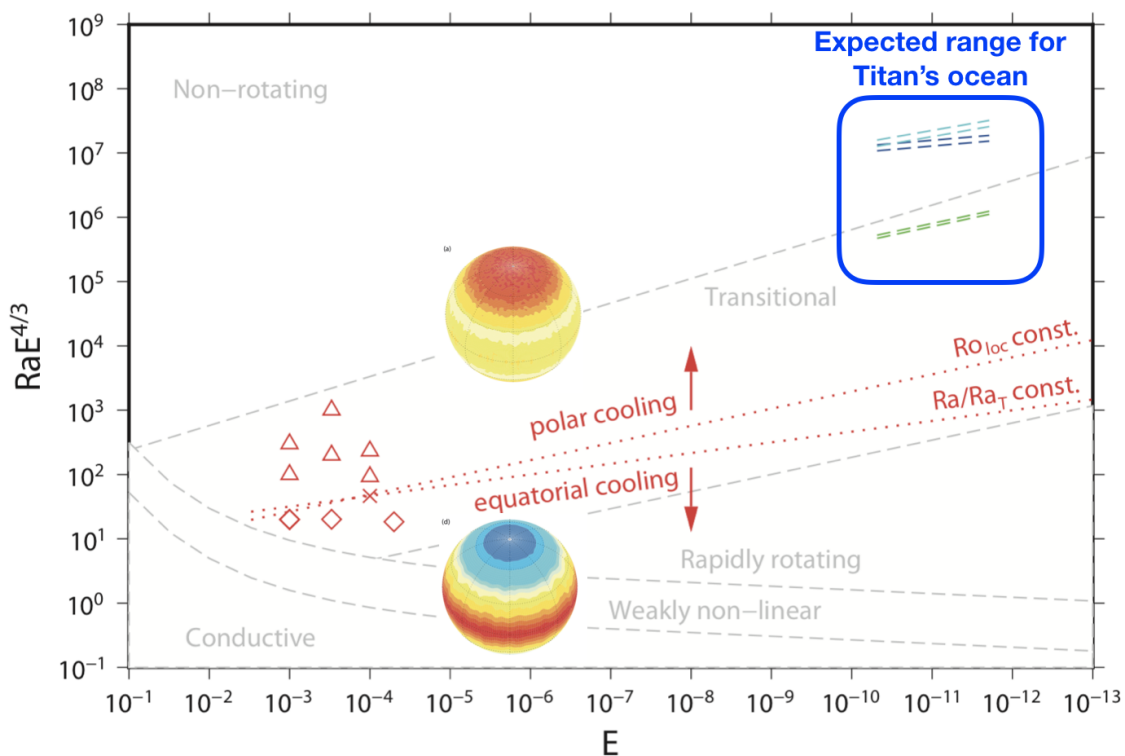
641

642 5.2 Dynamics of the ocean

643 Flows in Titan's subsurface ocean can be driven by thermo-compositional convection as well
644 as mechanically by tides (for a review, see Soderlund et al., 2020). For the rotating subsurface
645 oceans, the convective heat transfer efficiency and the outgoing heat flux pattern depend
646 strongly on the particular importance of driving buoyancy, Coriolis, and inertia forces when
647 compared to retarding viscous forces (e.g. Gastine et al., 2016; Soderlund et al., 2019; Amit
648 et al., 2020; Figure 7). Amit et al. (2020) described two distinct regimes - (i) equatorial cooling
649 characterized by a dominant top boundary heat flux in the equatorial region which was found
650 for cases when rotation was important, and (ii) polar cooling characterized by dominant top
651 boundary heat flux at polar regions found for cases when rotation was less important (see
652 Figure 7). The expected range of Ekman and Rayleigh numbers relevant to Titan's ocean (blue
653 box in Figure 7) suggests a rather limited effect of rotation on its dynamics, consistent with the
654 polar cooling pattern. These results are in agreement with the findings of Kvorka et al. (2018)
655 who predicted dominant heat fluxes at the poles to explain Titan's long-wavelength topography
656 (see also next section for more details). Using the same spectral code as Amit et al. (2020),
657 Soderlund (2019) found rather different results with the largest polar heat flux (i.e. polar
658 cooling) for cases with a strong influence of rotation and equatorial heat flux peaks (i.e.
659 equatorial cooling) for a more moderate rotational influence. This obvious contradiction
660 between their findings may be the result of different choice of mechanical boundary conditions
661 – while Soderlund (2019) prescribed impenetrable, stress-free boundaries, Amit et al. (2020)
662 used rigid boundaries. Similarly, the effect of thermal boundary conditions should be carefully
663 investigated since in both studies, isothermal boundaries were prescribed. However, given
664 that the ocean is sandwiched between two ice layers (HP ice layer below and ice I shell above)
665 with much slower dynamics, the incoming and outgoing heat flux are likely to be governed by
666 the dynamics of these two solid layers, i.e. a prescribed incoming and outgoing heat flux would
667 be a more appropriate boundary condition than prescribed temperature. A dedicated
668 numerical study investigating these different settings would certainly bring more insight into
669 the ocean dynamics of Titan as well as other ocean worlds.

670 Titan's eccentric orbit and nonzero obliquity result in time-variable tidal forcing that drives
671 ocean flow. For Europa, the associated tidal dissipation was suggested as an important source

672 of energy by Tyler (2008) although the assumed value of tidal quality factor remained
 673 debatable. To provide an independent constraint on the possible amount of ocean tidal
 674 dissipation, Chen et al. (2014) used the shallow-water equations that neglect the radial ocean
 675 currents with respect to horizontal currents (making the problem a two-dimensional one) with
 676 an Earth-like value of bottom drag coefficient. They also neglected the effect of the overlying
 677 ice shell. Their results show that the dissipated power in Titan's ocean due to obliquity tides is
 678 on the order of 10 GW, which was later confirmed by Hay & Matsuyama (2017). The
 679 corresponding surface heat flux of about 0.1 mW/m² is however negligible compared to the
 680 tidal heating in solid layers as well as to the radiogenic heating in the core (Chen et al., 2014,
 681 see also Section 4). The inclusion of the outer ice shell covering the ocean has a minor effect
 682 on both, the eccentricity and obliquity tidal heating in Titan's ocean. Recently, Rovira-Navarro
 683 et al. (2019) and Requier et al. (2019) performed simulations tailored to Europa and Enceladus
 684 that took into account the three-dimensional nature of ocean flows. Although the observed
 685 pattern of periodic inertial waves differed from the shallow-water results, the tidal dissipation
 686 due to these inertial waves was found negligible when compared to the traditional heat
 687 sources. Finally, let us note that future studies should also investigate the interaction between
 688 convection and the tidally-driven flows (Soderlund et al., 2020).
 689



690
 691 **Figure 7:** Regime diagram proposed by Gastine et al. (2016) showing the different regimes
 692 for convecting rotating flows in a spherical shell depending on Ekman number (E , ratio of
 693 viscous and Coriolis forces) and product of Rayleigh number and **Ekman number to the 4/3**
 694 ~~Ekman and Rayleigh numbers~~ (Ra , ratio of thermal buoyancy to momentum and heat
 695 diffusion). The blue box highlights the expected values for Titan's ocean (dashed colored lines,
 696 see Amit et al., 2020, for more details). Results by Amit et al. (2020) are denoted by red
 697 diamonds (equatorial cooling) and red triangles (polar cooling). The inserted spheres depict
 698 the long-term time-averaged heat flux anomaly (i.e. heat flux with respect to the mean value)

699 across the ocean top boundary. Red/blue denote positive/negative heat flux anomaly,
700 respectively. Modified from Amit et al. (2020).

701

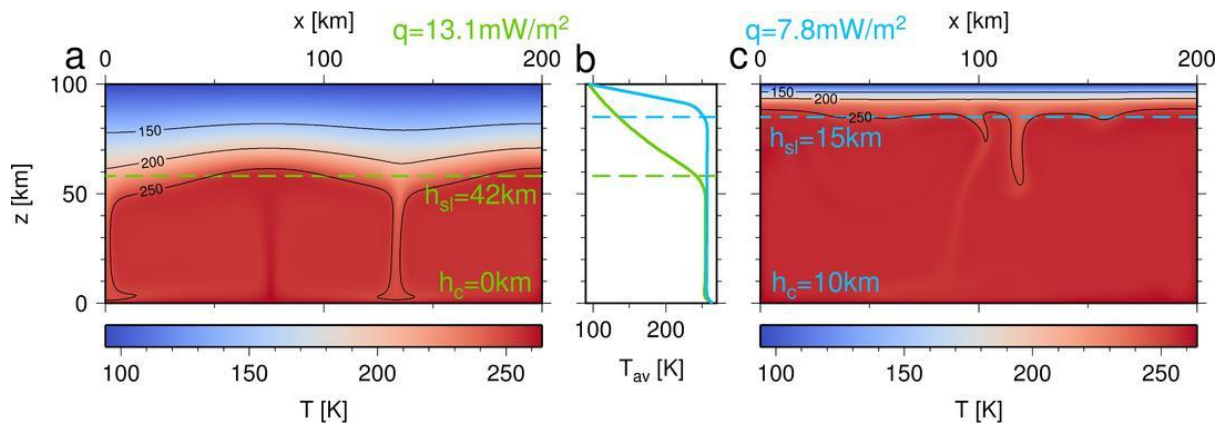
702 **5.3 Dynamics of the outer ice shell**

703 The thermal state of Titan's outer ice shell is not well constrained. Depending on its thickness
704 and the ice viscosity, heat can be transferred either by conduction (thin shells, large viscosity)
705 or convection (thick shells, small viscosity). The viscosity is mainly determined by the ice grain
706 size (Durham et al., 2001; Goldsby & Kohlstedt, 2001) which may vary from less than 1 mm
707 to more than a few mm and would evolve dynamically (Barr & McKinnon, 2007). Therefore,
708 the critical thickness for the convection to occur depends mainly on the ice grain size, often
709 represented by the viscosity value at the melting temperature, η_0 . Lefevre et al. (2014) found
710 that Titan's 100 km thick ice shell is likely to convect unless $\eta_0 \geq 3 \times 10^{16}$ Pa s, roughly
711 corresponding to a 7 mm grain size. If the shell is 50 km thick, the threshold viscosity would
712 be about one order of magnitude smaller, corresponding to a 3 mm grain size. The heat
713 transfer by convection is far more efficient than the conductive cooling and leads to an efficient
714 crystallization of the deep ocean unless another mechanism is acting to delay the freezing.

715

716 The presence of ammonia has been suggested (e.g., Grasset & Sotin, 1996) that would
717 decrease the ocean temperature, thus increasing viscosity and making convection less
718 efficient or not occurring at all. However, a significant ammonia concentration would be
719 necessary to substantially decrease the ocean temperature which is not compatible with the
720 densities inferred by Mitri et al. (2014) as well as with the recent work by Leitner & Lunine
721 (2020) who suggest that only up to about 5% of ammonia could be present in Titan's ocean.
722 Another possibility is tidal heating in the ice shell or the core that keeps oceans liquid in bodies
723 such as Europa or Enceladus (Tobie et al., 2005b; Choblet et al., 2017b). However, given the
724 high value of Titan's eccentricity and no resonance to maintain it on geological timescales, it
725 is not likely that significant dissipation is currently occurring in Titan's interior (Tobie et al.,
726 2005b) although more energy could have been dissipated earlier in the evolution (Section 4).
727 Alternatively, a crust made of methane clathrates - that have about ten times smaller thermal
728 conductivity than ice under Titan's surface conditions (Sloan et al., 2007) - has been proposed
729 to insulate Titan's interior and delay the ocean crystallization (e.g. Loveday et al., 2001; Tobie
730 et al., 2006). Recently, Kalousova & Sotin (2020b) revisited this concept and performed
731 simulations of thermal convection in Titan's clathrate capped ice shell. Figure 8 shows the
732 comparison of temperature for simulations without clathrates (panel a) and with a 10km thick
733 clathrate crust (panel c). The middle panel (b) shows the average temperature profiles for
734 these two cases. The inclusion of the clathrate crust results in: (i) a significant reduction of the
735 stagnant lid thickness (h_{sl} , dashed lines) - in this particular setting from 42km ($h_c=0$ km) to 15km
736 ($h_c=10$ km), and (ii) a substantial decrease in the amount of heat extracted from Titan's ocean
737 (q) - for the depicted case by about 40%. As a consequence of the thinner stagnant lid, a warm
738 material is brought closer to Titan's surface which may facilitate material exchange with the
739 surface e.g. due to cryovolcanism (Mitri et al., 2008; Lopes et al., 2013).

740



741
742

743 **Figure 8:** Comparison of temperature fields assuming a clathrate crust 0km (a) and 10km (c)
744 thick. Panel (b) shows the average temperature profiles (full lines). The dashed lines indicate
745 the stagnant lid (h_{sl}). Adapted from Kalousová & Sotin (2020b).

746

747 As discussed in Section 2, Titan's long wavelength topography is characterized by polar
748 depressions of about 300m and the negligible correlation of topography with the gravity field
749 anomalies points to a high degree of compensation (Durante et al., 2019). To explain the
750 observed topography, a concept of isostasy has been considered. Nimmo & Bills (2010)
751 assumed that Titan's shell is rigid and conductive and proposed that lateral ice shell thickness
752 variations (corresponding to Airy isostasy) can lead to topographies that fit well in the
753 observations (Figure 9a). The topic was further investigated by Lefevre et al. (2014) and
754 Kvorka et al. (2018) who found that lateral flows driven by the shell thickness variations would
755 tend to remove any ice shell/ocean interface topography unless the ice viscosity at the base

756 of the shell exceeds 10^{16} Pa s, corresponding to either coarse grain (\geq several mm) or very

757 cold ocean (≤ 240 K). As discussed above, such a cold ocean is not compatible with the high

758 value of k_2 (Section 3). Kvorka et al. (2018) further showed that Titan's topography cannot be
759 reproduced by the pattern of tidal heating in the ice shell as initially proposed by Nimmo & Bills

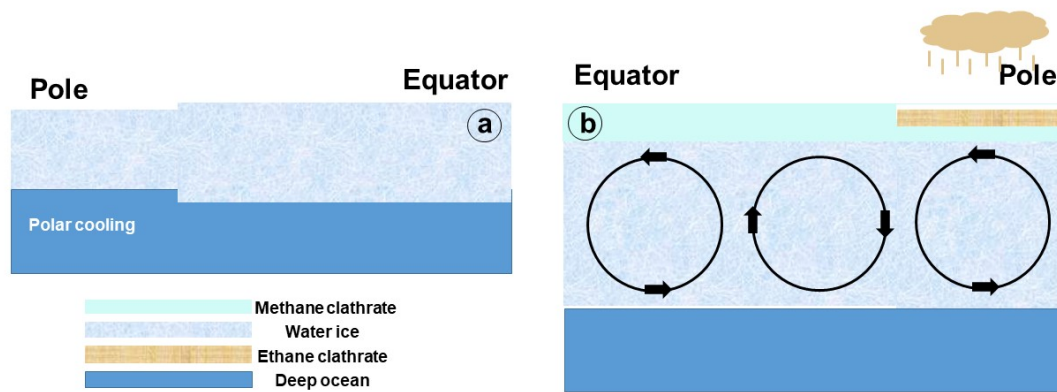
760 (2010). Their results however indicated that Titan's polar flattening could be explained by
761 lateral variations of ocean heat flux with amplitudes between 0.1 and 1 mW/m^2 , warm water
762 upwellings at the poles and cold downwellings close to the equator. Such a pattern would
763 agree with the polar cooling of Amit et al. (2020) (see previous section). Alternatively,

764 Choukroun & Sotin (2012) proposed that the polar depressions could be explained by
765 subsidence due to the presence of ethane clathrate that is about 8% denser than water ice
766 (corresponding to Pratt isostasy, Figure 9b). This model is supported by the observation of
767 ethane rains at the poles (Griffith et al., 2006). The ethane polar caps would be the ethane

768 reservoir that could explain the absence of atmospheric ethane although it is the main product
769 of methane photolysis in the upper atmosphere (e.g. Lavvas et al., 2008). The ethane clathrate
770 would form by substitution of methane by ethane in the methane clathrate crust, a process

771 observed in laboratory experiments (Murshed et al., 2010) or by the reaction of liquid ethane
772 with water ice as observed experimentally by Vu et al. (2020).

773



774
775

776 **Figure 9:** Models of ice I shell that can explain the observed gravity and topography data: (a)
777 Airy model (Nimmo & Bills, 2010), (b) Pratt model (Choukroun & Sotin, 2012).
778

779 **5.4 Coupled evolution of the hydrosphere and implications for the atmosphere**

780 As stated in Mitchell and Lora (2016), models need to consider the interactions between
781 Titan's atmosphere, surface, and subsurface in order to make further progress in
782 understanding Titan's complex climate system. The greatest mystery is how can Titan retain
783 an abundance of atmospheric methane with only limited surface liquids, while methane is
784 being irreversibly destroyed by photochemistry. A related mystery is how can Titan hide all
785 ethane that is produced in this process (Lavvas et al., 2008). All along Titan's history, the
786 evolution of the hydrosphere has likely influenced the composition of the atmosphere, by
787 controlling the outgassing rate (e.g. Tobie et al., 2006) and possible internal recycling of
788 hydrocarbon compounds (e.g. Choukroun and Sotin, 2012). The hydrosphere may contain
789 large quantities of volatiles, either dissolved in the ocean or stored in the form of gas clathrate
790 hydrates in the icy shell (Tobie et al., 2012; Choukroun et al., 2010, 2013).
791

792 The release of these volatile compounds is, however, limited due to their solubility in the
793 internal ocean and the clathration processes within the H₂O layers. Outgassing from the
794 interior may occur through two different mechanisms: (1) destabilization of clathrates stored
795 in the outer ice shell by thermal convective plumes or by impacts, (2) mobilization of dissolved
796 gas molecules contained in the water ocean and subsequent bubble formation if the ocean
797 gets saturated (Tobie et al., 2006; 2009). Both processes are controlled by methane, since it
798 is expected to be the dominant gas in the form of clathrate hydrate in the crust and since it is
799 the only gas compound that may reach the saturation point in the ocean during periods of
800 reduced ice shell thicknesses. The amount of ⁴⁰Ar detected in the atmosphere provides
801 constraints on the level of methane outgassing through time. Owing to its low solubility in
802 water, argon should be preferentially incorporated in CH₄-rich bubbles when they form at the
803 ocean-ice interface and should then be transported upwards by the percolating CH₄-rich fluids.
804 Following this extraction mechanism, Tobie et al. (2012) estimated that the atmospheric mass
805 of methane has been renewed at least 20-30 times during Titan's evolution in order to explain
806 the atmospheric abundance of ⁴⁰Ar as detected by Huygens (Niemann et al., 2010).

807 Following the evolution scenario proposed by Tobie et al. (2006), the outgassing of methane
808 may result in episodic destabilization of the methane clathrate reservoir, accumulated in the
809 crust during the differentiation process. This crust would then thin in response to the release
810 of heat associated with the core evolution (Tobie et al., 2006), resulting in the dissolution of

811 methane in the ocean and the outgassing of the gas in excess (Tobie et al., 2009). According
812 to this scenario, several kilometers of methane clathrates may still be present in the outer icy
813 shell, limiting the cooling rate of the ocean (Kalousová & Sotin, 2020b). Recent thermal
814 destabilizations of this reservoir may explain the present-day atmospheric methane (Tobie et
815 al., 2006). This evolution model was based on a simplified 1D approach, assuming an
816 ammonia-water ocean and ignoring the coupling between the ocean and the high-pressure
817 ice layer. More sophisticated evolution models taking into account the latest advances in
818 physical and thermodynamic description of the hydrosphere should be developed to better
819 understand the impact of the hydrosphere evolution on the atmosphere. The recent advances
820 made in the description of the large-scale dynamics of the high-pressure ice layer (Section
821 5.1) and of the ocean (Section 5.2) motivate the need for developing a new generation of
822 models describing the exchange processes between the different layers in a 3D framework
823 and using a consistent thermodynamic approach for phase changes and chemical exchanges
824 between each layer of the hydrosphere.

825

826 **6. Discussion and conclusions**

827 The Cassini-Huygens mission has provided key information on Titan's interior structure such
828 as the presence of a deep ocean, the near hydrostatic equilibrium of its long wavelength
829 topography, and the low density of its rocky core. Titan is almost the same size and mass as
830 Ganymede, Jupiter's largest moon but the apparent absence of an inner iron-rich core seems
831 to indicate that Titan did not experience as high temperatures in its rocky core as Ganymede.
832 The upcoming JUICE mission managed by the European Space Agency (launch expected in
833 2022) will orbit Ganymede and will provide a unique set of gravity, topography, rotation,
834 electro-magnetic field, and radar sounder measurements. These data will provide a very good
835 picture of Ganymede's interior structure. The comparison between the two moons may help
836 understand the interior structure and thermal evolution of each of them.

837

838 The habitability requirements for a planet or a moon include water, essential elements
839 (CHNOPS), chemical energy, and time (Cockell et al., 2016). The Cassini-Huygens mission
840 demonstrated that Titan has a deep ocean. The thermal evolution included several episodes
841 when water and rocks interacted and most likely left elements in the ocean. Organic material
842 forms in the atmosphere and after falling on the surface, it may be transferred to the deep
843 ocean. As discussed in Section 2.4 (Atmospheric constraints) and in Section 5.1 (HP ice layer
844 dynamics), exchanges have occurred between the rocky core and the atmosphere, implying
845 that transfer of volatiles and other elements coming from the decomposition of IOM in the core
846 have existed between the rocky core and the ocean. Whether the transfer from the surface to
847 the ocean and the transfer from the rocky core to the ocean can provide the chemical
848 disequilibrium and chemical energy that could lead to life is an open issue.

849

850 Models describing the geological evolution of Titan must take into account all the information
851 that has been acquired with the Cassini-Huygens data as well as the results of laboratory
852 experiments. Tobie et al. (2006) proposed a model that was consistent with the amount of
853 methane in the atmosphere, the presence of a deep ocean, the large eccentricity, and the
854 mass. New information from Cassini, the recent progress on EoS and other key parameters
855 of the compounds that built Titan, as well as recent advances in the modelling of multi-phase
856 layers point to the development of a new thermal evolution model. Such a model would be
857 useful to define questions that could be answered by the upcoming Dragonfly mission (Turtle
858 et al., 2017). Questions such as the presence or not of a clathrate crust, the thickness of the

859 ice shell, the tectonic activity of Titan may be answered thanks to the geophysical package
860 onboard that mission (Lorenz et al., 2019). It will shed more light on Titan, the satellite that
861 resembles the Earth more than any other.

862

863 **Acknowledgements**

864 Part of this work was carried out at the Jet Propulsion Laboratory, California Institute of
865 Technology, under a contract with the National Aeronautics and Space Administration. This
866 work was partially supported by the NASA Astrobiology Institute through its JPL-led team
867 entitled Habitability of Hydrocarbon Worlds: Titan and Beyond (17-NAI8_2-0017). K.K. was
868 supported by the Czech Science Foundation through project No. 19-10809S and by Charles
869 University Research Program No. UNCE/SCI/023. G.T. acknowledges support from the
870 French "Agence Nationale de Recherche" A.N.R. (OASIS project, ANR-16-CE31-0023-
871 01). Copyright ©2020 All rights reserved.

872

873 **References**

- 874 - Amit, H., Choblet, G., Tobie, G., Terra-Nova, F., Čadek, O., & Bouffard, M. (2020).
875 Cooling patterns in rotating thin spherical shells - Application to Titan's subsurface
876 ocean. *Icarus*, 338, 113509. <https://doi.org/10.1016/j.icarus.2019.113509>.
- 877 - Baland, R.-M., Van Hoolst, T., Yseboodt, M., & Karatekin, Ö. (2011). Titan's obliquity
878 as evidence of a subsurface ocean? *Astron. Astrophys.*, 530, A141.
879 <http://doi.org/10.1051/0004-6361/201116578>.
- 880 - Baland, R.-M., Tobie, G., Lefevre, A., & Van Hoolst, T. (2014). Titan's internal structure
881 inferred from its gravity field, shape, and rotation state. *Icarus*, 237, 29–41.
882 <https://doi.org/10.1016/j.icarus.2014.04.007>.
- 883 - Barnes, J. W., Brown, R. H., Radebaugh, J., Buratti, B. J., Sotin, C., Le Mouelic, S.,
884 Rodriguez, S., Turtle, E. P., Perry, J., Clark, R., Baines, K. H., & Nicholson, P. D.
885 (2006). Cassini observations of flow-like features in western Tui Regio, Titan.
886 *Geophys. Res. Lett.*, 33(16), L16204. <http://doi.org/10.1029/2006GL026843>.
- 887 - Barr, A. C., Citron, R. I., & Canup, R. M. (2010). Origin of a partially differentiated Titan.
888 *Icarus*, 209(2), 858–862. <http://doi.org/10.1016/j.icarus.2010.05.028>.
- 889 - Barr, A. C., & McKinnon, W. B. (2007). Convection in ice I shells and mantles with self-
890 consistent grain size. *J. Geophys. Res. Planets*, 112(E2), E02012.
891 <http://doi.org/10.1029/2006JE002781>.
- 892 - Béghin, C., Simoes, F., Krasnoselskikh, V., Schwingenschuh, K., Berthelier, J. J.,
893 Besser, B. P., Bettanini, C., Gard, R., Hamelin, M., Lopez-Moreno, J. J., Molina-
894 Cuberos, G. J., & Tokano, T. (2007). A Schumann-like resonance on Titan driven by
895 Saturn's magnetosphere possibly revealed by the Huygens Probe. *Icarus*, 191(1), 251-
896 -266, <http://doi.org/10.1016/j.icarus.2007.04.005>.
- 897 - Béghin, C., Randriamboarison, O., Hamelin, M., Karkoschka, E., Sotin, C., Whitten, R.
898 C., Berthelier, J. J., Gard, R., & Simoes, F. (2012). Analytic theory of Titan's
899 Schumann resonance: Constraints on ionospheric conductivity and buried water
900 ocean. *Icarus*, 218(2), 1028–1042. <https://doi.org/10.1016/j.icarus.2012.02.005>.
- 901 - Bézard, B. (2014). The methane mole fraction in Titan's stratosphere from DISR
902 measurements during the Huygens probe's descent. *Icarus*, 242, 64–73,
903 <http://doi.org/10.1016/j.icarus.2014.07.013>.
- 904 - Bills, B. G., & Nimmo, F. (2008). Forced obliquity and moments of inertia of Titan.
905 *Icarus*, 196(1), 293–297. <http://doi.org/10.1016/j.icarus.2008.03.002>.

- 906 - Bills, B. G., & Nimmo, F. (2011). Rotational dynamics and internal structure of Titan.
 907 Icarus, 214(1), 351--355. <http://doi.org/10.1016/j.icarus.2011.04.028>.
- 908 - Bollengier, O., Brown, J. M., & Shaw, G. H. (2019). Thermodynamics of pure liquid
 909 water: Sound speed measurements to 700 MPa down to the freezing point, and an
 910 equation of state to 2300 MPa from 240 to 500 K. J. Chem. Phys., 151(5), 054501.
 911 <http://doi.org/10.1063/1.5097179>.
- 912 - Bonnet-Gibet V., Choblet G., Sotin C., Vance S.D., Guignard J. and Tobie G. (2020)
 913 Thermal and chemical evolution of Ganymede's primitive core; EPSC 2020.
- 914 - Brown, J. M. (2018). Local basis function representations of thermodynamic surfaces:
 915 Water at high pressure and temperature as an example. Fluid Phase Equilib., 463, 18-
 916 -31. <http://doi.org/10.1063/1.5097179>.
- 917 - Buono, A. S., & Walker, D. (2011). The Fe-rich liquidus in the Fe-FeS system from
 918 1 bar to 10 GPa. Geochim. Cosmochim. Acta, 75(8), 2072--2087.
 919 <http://doi.org/10.1016/j.gca.2011.01.030>.
- 920 - Castillo-Rogez, J.C., & Lunine, J.I. (2010). Evolution of Titan's rocky core constrained
 921 by Cassini observations. Geophys. Res. Lett., 37 (L20205).
 922 <https://doi.org/10.1029/2010GL044398>.
- 923 - Chen, E., Nimmo, F., & Glatzmaier, G. (2014). Tidal heating in icy satellite oceans.
 924 Icarus, 229, 11--30. <https://doi.org/10.1016/j.icarus.2013.10.024>.
- 925 - Choblet, G., Tobie, G., Sotin, C., Kalousová, K., & Grasset, O. (2017a). Heat transport
 926 in the high-pressure ice mantle of large icy moons, Icarus, 285, 252--262.
 927 <http://doi.org/10.1016/j.icarus.2016.12.002>.
- 928 - Choblet, G., Tobie, G., Sotin, C., Běhouňková, M., Čadek, O., Postberg, F., & Souček,
 929 O. (2017b). Powering prolonged hydrothermal activity inside Enceladus. Nat. Astron.,
 930 12, 841--847. <https://doi.org/10.1038/s41550-017-0289-8>.
- 931 - Choukroun, M., & Grasset, O. (2010). Thermodynamic data and modeling of the water
 932 and ammonia-water phase diagrams up to 2.2 GPa for planetary geophysics. J. Chem.
 933 Phys., 133(14), 133402. <http://doi.org/10.1063/1.3487520>.
- 934 - Choukroun, M., Grasset, O., Tobie, G., & Sotin, C. (2010). Stability of methane
 935 clathrate hydrates under pressure: Influence on outgassing processes of methane on
 936 Titan. Icarus, 205(2), 581--593. <https://doi.org/10.1016/j.icarus.2009.08.011>.
- 937 - Choukroun, M., & Sotin, C. (2012). Is Titan's shape caused by its meteorology and
 938 carbon cycle? Geophys. Res. Lett., 39, L04201.
 939 <https://doi.org/10.1029/2011GL050747>.
- 940 - Choukroun, M., Kieffer, S. W., Lu, X., & Tobie G. (2013). Clathrate Hydrates:
 941 Implications for Exchange Processes in the Outer Solar System. In: Gudipati, M., &
 942 Castillo-Rogez, J. (eds). The Science of Solar System Ices. Astrophysics and Space
 943 Science Library, vol 356. Springer, New York, NY.
- 944 - Cockell, C. S., Bush, T., Bryce, C., Direito, S., Fox-Powell, M., Harrison, J. P., Lammer,
 945 H., Landenmark, H., Martin-Torres, J., Nicholson, N., Noack, L., O'Malley-James, J.,
 946 Payler, S. J., Rushby, A., Samuels, T., Schwendner, P., Wadsworth, J., & Zorzano, M.
 947 P. (2016). Habitability: A Review. Astrobiology, 16(1), 89--117.
 948 <http://doi.org/10.1089/ast.2015.1295>.
- 949 - Connolly, J. A. D. (1990). Multivariable phase diagrams - an algorithm based on
 950 generalized thermodynamics. Am. J. Sci., 290(6), 666--718.
 951 <http://doi.org/10.2475/ajs.290.6.666>.
- 952 - Corlies, P., Hayes, A. G., Birch, S. P. D., Lorenz, R., Stiles, B. W., Kirk, R., Poggiali,
 953 V., Zebker, H., & less, L. (2017). Titan's topography and shape at the end of the

- 954 Cassini mission. *Geophys. Res. Lett.*, 44(23), 11754--11761.
955 <http://doi.org/10.1002/2017GL075518>.
- 956 - Croft, S. K. (1982). A first-order estimate of shock heating and vaporization in oceanic
957 impacts, in *Geological Implications of Impacts of Large Asteroids and Comets on*
958 *Earth*, edited by T. L. Silver and P. H. Schultz, *Spec. Pap. Geol. Soc. Am.*, 90, 143–
959 152.
- 960 - Croft, S. K., Lunine, J. I., & Kargel, J. (1988). Equation of state of ammonia-water
961 liquid: derivation and planetological applications. *Icarus*, 73(2), 279--293.
962 [http://doi.org/10.1016/0019-1035\(88\)90098-X](http://doi.org/10.1016/0019-1035(88)90098-X).
- 963 - Durante, D., Hemingway, D., Racioppa, P., Iess, L., & Stevenson, D. (2019). Titan's
964 gravity field and interior structure after Cassini. *Icarus*, 326, 123–132.
965 <https://doi.org/10.1016/j.icarus.2019.03.003>.
- 966 - Durham, W.B., & Stern, L.A. (2001). Rheological properties of water ice - applications
967 to satellites of the outer planets. *Annu. Rev. Earth Planet. Sci.*, 29, 295–330.
968 <https://doi.org/10.1146/annurev.earth.29.1.295>.
- 969 - Durham, W.B., Stern, L.A., & Kirby, S.H. (1996). Rheology of water ices V and VI. *J.*
970 *Geo-phys. Res. Solid Earth*, 101(B2), 2989–3001. <https://doi.org/10.1029/95JB03542>.
- 971 - Durham, W.B., Stern, L.A., & Kirby, S.H. (1997). Creep of water ices at planetary
972 conditions: a compilation. *J. Geophys. Res. Planets*, 102(E7), 16293–16302.
973 <https://doi.org/10.1029/97JE00916>.
- 974 - Elachi, C., Allison, M. D., Borgarelli, L., Encrenaz, P., Im, E., Janssen, M. A., Johnson,
975 W. T. K., Kirk, R. L., Lorenz, R. D., Lunine, J. I., Muhleman, D. O., Ostro, S. J., Picardi,
976 G., Posa, F., Rapley, C. G., Roth, L. E., Seu, R., Soderblom, L. A., Vetrilla, S., Wall,
977 S. D., Wood, C. A., & Zebker, H. A. (2004). Radar: The Cassini Titan RADAR Mapper.
978 *Space Sci. Rev.*, 115(1-4), 71--110. <http://doi.org/10.1007/s11214-004-1438-9>.
- 979 - Fischer, G., & Gurnett, D.A. (2011). The search for Titan lightning radio emissions.
980 *Geophys. Res. Lett.*, 38, L08206. <https://doi.org/10.1029/2011GL047316>.
- 981 - Fortes, A. D., Grindrod, P. M., Trickett, S. K., & Vočadlo, L. (2007), Ammonium sulfate
982 on Titan: Possible origin and role in cryovolcanism. *Icarus*, 188(1), 139--153.
983 <http://doi.org/10.1016/j.icarus.2006.11.002>.
- 984 - Fortes, A. D. (2012). Titan's internal structure and the evolutionary consequences.
985 *Planet. Space Sci.*, 60(1), 10–17. <https://doi.org/10.1016/j.pss.2011.04.010>.
- 986 - Friedson, A. J., & Stevenson, D. J. (1983). Viscosity of rock mixtures and applications
987 to the evolution of icy satellites. *Icarus*, 56(1), 1--14. [http://doi.org/10.1016/0019-1035\(83\)90124-0](http://doi.org/10.1016/0019-1035(83)90124-0).
- 988 - Gao, P., & Stevenson, D.J. (2013). Nonhydrostatic effects and the determination of icy
989 satellites' moment of inertia. *Icarus*, 226(2), 1185--1191.
990 <https://doi.org/10.1016/j.icarus.2013.07.034>.
- 991 - Gastine, T., Wicht, W., & Aubert, J. (2016), Scaling regimes in spherical shell rotating
992 convection, *J. Fluid Mech.*, 808, 690-732. <https://doi.org/10.1017/jfm.2016.659>.
- 993 - Glein, C. R. (2015). Noble gases, nitrogen, and methane from the deep interior to the
994 atmosphere of Titan. *Icarus*, 250, 570--586,
995 <http://doi.org/10.1016/j.icarus.2015.01.001>.
- 996 - Goldsby, D. L., & Kohlstedt, D. L. (2001). Superplastic deformation of ice:
997 Experimental observations. *J. Geophys. Res.*, 106(B6), 11,017--11,030.
998 <https://doi.org/10.1029/2000JB900336>.
- 999

- 1000 - Grasset, O., & Pargamin, J. (2005). The ammonia-water system at high pressures:
1001 Implications for the methane of Titan. *Planet. Space Sci.*, 53(4), 371–384.
1002 <http://doi.org/10.1016/j.pss.2004.09.062>.
- 1003 - Grasset, O., & Sotin, C. (1996). The cooling rate of a liquid shell in Titan's interior.
1004 *Icarus*, 123(1), 101–112. <https://doi.org/10.1006/icar.1996.0144>.
- 1005 - Griffith, C. A., Penteadó, P., Rannou, P., Brown, R., Boudon, V., Baines, K. H., Clark,
1006 R., Drossart, P., Buratti, B., Nicholson, P., McKay, C. P., Coustenis, A., Negrao, A., &
1007 Jaumann, R. (2006). Evidence for a polar ethane cloud on Titan. *Science*, 313(5793),
1008 1620–1622, <http://doi.org/10.1126/science.1128245>.
- 1009 - Griffith, C., Mitchell, J. L., Lavvas, P., & Tobie, G. (2013). Titan's evolving climate.
1010 *Comparative Climatology of Terrestrial Planets*, 1-27.
- 1011 ~~Griffith, C., Rafkin, S., Rannou, P., & McKay, C. (2014). Storms, clouds, and weather,~~
1012 ~~in *Titan: Interior, Surface, Atmosphere, and Space Environment*, edited by I. Müller-~~
1013 ~~Wedarg et al., Cambridge Univ. Press, Cambridge, U. K.~~
- 1014 - Griffith, C. A., Penteadó, P. F., Turner, J. D., Neish, C. D., Mitri, G., Montiel, N. J.,
1015 Schoenfeld, A., & Lopes, R. M. C. (2019). A corridor of exposed ice-rich bedrock
1016 across Titan's tropical region. *Nat. Astron.*, 3(7), 642–648.
1017 <http://doi.org/10.1038/s41550-019-0756-5>.
- 1018 - Hay, H. C. F. C., & Matsuyama, I. (2017). Numerically modelling tidal dissipation with
1019 bottom drag in the oceans of Titan and Enceladus. *Icarus*, 281, 342–356.
1020 <http://doi.org/10.1016/j.icarus.2016.09.022>.
- 1021 - Hilairet, N., Reynard, B., Wang, Y. B., Daniel, I., Merkel, S., Nishiyama, N., &
1022 Petitgirard, S. (2007). High-pressure creep of serpentine, interseismic deformation,
1023 and initiation of subduction. *Science*, 318(5858), 1910–1913.
1024 <http://doi.org/10.1126/science.1148494>.
- 1025 - Hogenboom, D. L., Kargel, J. S., Consolmagno, G. J., Holden, T. C., Lee, L.,
1026 Buyyounouski, M. (1997). The ammonia-water system and the chemical differentiation
1027 of icy satellites. *Icarus*, 128(1), 171–180. <http://doi.org/10.1006/icar.1997.5705>.
- 1028 - Hörst, S. M. (2017). Titan's atmosphere and climate. *J. Geophys. Res. Planets*, 122(3),
1029 432–482, <http://doi.org/10.1002/2016JE005240>.
- 1030 - Hussmann, H., Choblet, G., Lainey, V., Matson, D. L., Sotin, C., Tobie, G., & Van
1031 Hoolst, T. (2010). Implications of Rotation, Orbital States, Energy Sources, and Heat
1032 Transport for Internal Processes in Icy Satellites, *Space Sci. Rev.*, 153(1-4), 317–348,
1033 <http://doi.org/10.1007/s11214-010-9636-0>.
- 1034 - Iess, L., Rappaport, N.J., Jacobson, R.A., Racioppa, P., Stevenson, D.J., Tortora, P.,
1035 Arm-strong, J.W., & Asmar, S.W. (2010). Gravity field, shape, and moment of inertia
1036 of Titan. *Science*, 327 (5971), 1367–1369. <https://doi.org/10.1126/science.1182583>.
- 1037 - Iess, L., Jacobson, R. A., Ducci, M., Stevenson, D. J., Lunine, J. I., Armstrong, J. W.,
1038 Asmar, S. W., Racioppa, P., Rappaport, N. J., Tortora, P. (2012). The tides of Titan.
1039 *Science*, 337(6093), 457–459. <https://doi.org/10.1126/science.1219631>.
- 1040 - Jaumann, R., Brown, R. H., Stephan, K., Barnes, J. W., Soderblom, L. A., Sotin, C.,
1041 Le Mouelic, S., Clark, R. N., Soderblom, J., Buratti, B. J., Wagner, R., McCord, T. B.,
1042 Rodriguez, S., Baines, K. H., Cruikshank, D. P., Nicholson, P. D., Griffith, C. A.,
1043 Langhans, M., & Lorenz, R. D. (2008). Fluvial erosion and post-erosional processes
1044 on Titan. *Icarus*, 197(2), 526–538. <http://doi.org/10.1016/j.icarus.2008.06.002>.
- 1045 - Journaux, B., Kalousová, K., Sotin, C., Tobie, G., Vance, S., Saur, J., Bollengier, O.,
1046 Noack, L., Ruckriemen-Bez, T., Van Hoolst, T., Soderlund, K. M., & Brown, J. M.

- 1047 (2020a), Large ocean worlds with high-pressure ices, *Space Sci. Rev.*, 216(7),
1048 <http://doi.org/10.1007/s11214-019-0633-7>.
- 1049 - Journaux, B., Brown, J. M., Pakhomova, A., Collings, I. E., Petitgirard, S., Espinoza,
1050 P., Ballaran, T. B., Vance, S. D., Ott, J., Cova, F., Garbarino, G., Hanfland, M. (2020b).
1051 Holistic approach for studying planetary hydrospheres: Gibbs representation of ices
1052 thermodynamics, elasticity, and the water phase diagram to 2,300 MPa. *J. Geophys.*
1053 *Res. Planets*, 125(1), e2019JE006176, <http://doi.org/10.1029/2019JE006176>.
- 1054 - Kalousová, K., & Sotin, C. (2018). Melting in high-pressure ice layers of large ocean
1055 worlds – implications for volatiles transport. *Geophys. Res. Lett.*, 45(16), 8096–8103.
1056 <https://doi.org/10.1029/2018GL078889>.
- 1057 - Kalousová, K., Sotin, C., Choblet, G., Tobie, G., & Grasset, O. (2018). Two-phase con-
1058 vection in Ganymede's high-pressure ice layer – implications for its geological
1059 evolution. *Icarus*, 299, 133–147. <https://doi.org/10.1016/j.icarus.2017.07.018>.
- 1060 - Kalousová, K., & Sotin, C. (2020a). Dynamics of Titan's high-pressure ice layer, *Earth*
1061 *Planet. Sci. Lett.*, 545, 116416, <http://doi.org/10.1016/j.epsl.2020.116416>.
- 1062 - Kalousová, K., & Sotin, C. (2020b). The insulating effect of methane clathrate crust on
1063 Titan's thermal evolution, *Geophys. Res. Lett.*, 47(13), e2020GL087481,
1064 <http://doi.org/10.1029/2020GL087481>.
- 1065 - Khurana, K. K., Kivelson, M. G., Stevenson, D. J., Schubert, G., Russell, C. T., Walker,
1066 R. J., & Polanskey, C. (1998). Induced magnetic fields as evidence for subsurface
1067 oceans in Europa and Callisto. *Nature*, 395(6704), 777–780.
1068 <http://doi.org/10.1038/27394>.
- 1069 - Kirk, R. L., & Stevenson, D. J. (1987). Thermal evolution of a differentiated Ganymede
1070 and implications for surface features. *Icarus*, 69(1), 91–134.
1071 [http://doi.org/10.1016/0019-1035\(87\)90009-1](http://doi.org/10.1016/0019-1035(87)90009-1).
- 1072 - Kirk, R. L., Howington-Kraus, E., Redding, B., Aharonson, O., Bills, B.G., Hayes, A.
1073 G., Iess, L., Lopes, R. M. C., Lorenz, R. D., Lucas, A., Lunine, J. I., Meriggiola, R.,
1074 Mitchell, K. L., Neish, C. D., Radebaugh, J., Stiles, B. W., Stofan, E. R., Wall, S. D., &
1075 Wood, C. A. (2013). Topographic mapping of Titan: Completion of a global
1076 radargrammetric control network opens the floodgates for stereo DTM production.
1077 44th Lunar and Planetary Science Conference, Texas, 2898.
- 1078 - Kivelson, M. G., Khurana, K. K., Russell, C. T., Walker, R. J., Warnecke, J., Coroniti,
1079 F. V., Polanskey, C., Southwood, D. J., & Schubert, G. (1996). Discovery of
1080 Ganymede's magnetic field by the Galileo spacecraft. *Nature*, 384(6609), 537–541.
1081 <http://doi.org/10.1038/384537a0>.
- 1082 - Kivelson, M. G., Khurana, K. K., & Volwerk, M. (2002). The permanent and inductive
1083 magnetic moments of Ganymede. *Icarus*, 157(2), 507–522.
1084 <http://doi.org/10.1006/icar.2002.6834>.
- 1085 - Kruijjer, T. S., Burkhardt, C., Budde, G., & Kleine, T. (2017). Age of Jupiter inferred
1086 from the distinct genetics and formation times of meteorites. *Proc. Natl. Acad. Sci.*
1087 *U.S.A.*, 114(26), 6712–6716, <http://doi.org/10.1073/pnas.1704461114>.
- 1088 - Kuramoto, K., & Matsui, T. (1994). Formation of a hot proto-atmosphere on the
1089 accreting giant icy satellite: Implications for the origin and evolution of Titan,
1090 Ganymede, and Callisto. *J. Geophys. Res. Planets*, 99(E10), 21183–21200,
1091 <http://doi.org/10.1029/94JE01864>.
- 1092 - Kvorka, J., Čadek, O., Tobie, G., Choblet, G. (2018). Does Titan's long-wavelength
1093 topography contain information about subsurface ocean dynamics? *Icarus*, 310, 149-
1094 -164. <http://doi.org/10.1016/j.icarus.2017.12.010>.

- 1095 - Lainey, V., Casajus, L. G., Fuller, J., Zannoni, M., Tortora, P., Cooper, N., Murray, C.,
1096 Modenini, D., Park, R. S., Robert, V., Zhang, Q. F. (2020). Resonance locking in giant
1097 planets indicated by the rapid orbital expansion of Titan. *Nat. Astron.*,
1098 <http://doi.org/10.1038/s41550-020-1120-5>.
- 1099 - Lavvas, P. P., Coustenis, A., & Vardavas, I. M. (2008). Coupling photochemistry with
1100 haze formation in Titan's atmosphere, Part II: Results and validation with
1101 Cassini/Huygens data. *Planet. Space Sci.*, 56(1), 67--99.
1102 <http://doi.org/10.1016/j.pss.2007.05.027>.
- 1103 - Lefevre, A., Tobie, G., Choblet, G., & Čadek, O. (2014). Structure and dynamics of
1104 Titan's outer icy shell constrained from Cassini data. *Icarus*, 237, 16--28.
1105 <http://doi.org/10.1016/j.icarus.2014.04.006>.
- 1106 - Leitner, M. A., & Lunine, J. I. (2019). Modeling early Titan's ocean composition. *Icarus*,
1107 333, 61--70. <https://doi.org/10.1016/j.icarus.2019.05.008>.
- 1108 - Le Mouelic, S., Paillou, P., Janssen, M. A., Barnes, J. W., Rodriguez, S., Sotin, C.,
1109 Brown, R. H., Baines, K. H., Buratti, B. J., Clark, R. N., Crapeau, M., Encrenaz, P. J.,
1110 Jaumann, R., Geudtner, D., Paganelli, F., Soderblom, L., Tobie, G., & Wall, S. (2008).
1111 Mapping and interpretation of Sinlap crater on Titan using Cassini VIMS and RADAR
1112 data. *J. Geophys. Res. Planets*, 113(E4), E04003.
1113 <http://doi.org/10.1029/2007JE002965>.
- 1114 - Le Mouelic, S., Cornet, T., Rodriguez, S., Sotin, C., Seignovert, B., Barnes, J. W.,
1115 Brown, R. H., Baines, K. H., Buratti, B. J., Clark, R. N., Nicholson, P. D., Lasue, J.,
1116 Pasek, V., Soderblom, J. M. (2019). The Cassini VIMS archive of Titan: From browse
1117 products to global infrared color maps. *Icarus*, 319, 121--132,
1118 <http://doi.org/10.1016/j.icarus.2018.09.017>.
- 1119 - Lopes, R. M. C., Kirk, R. L., Mitchell, K. L., LeGall, A., Barnes, J. W., Hayes, A., Kargel,
1120 J., Wye, L., Radebaugh, J., Stofan, E. R., Janssen, M. A., Neish, C. D., Wall, S. D.,
1121 Wood, C. A., Lunine, J. I., & Malaska, M. J. (2013). Cryovolcanism on Titan: New
1122 results from Cassini RADAR and VIMS. *J. Geophys. Res. Planets*, 118, 416--435.
1123 <https://doi.org/10.1002/jgre.20062>.
- 1124 - Lorenz, R. D., & Le Gall, A. (2020). Schumann resonance on Titan: A critical Re-
1125 assessment. *Icarus*, 351, 113942. <http://doi.org/10.1016/j.icarus.2020.113942>.
- 1126 - Lorenz, R. D., Stiles, B. W., Kirk, R. L., Allison, M. D., del Marmo, P. P., Iess, L.,
1127 Lunine, J. I., Ostro, S. J., Hensley, S. (2008). Titan's rotation reveals an internal ocean
1128 and changing zonal winds. *Science*, 319(5870), 1649--1651.
1129 <http://doi.org/10.1126/science.1151639>.
- 1130 - Lorenz, R.D., Panning, M., Staehler, S.C., Shiraishi, H., Yamada, R., & Turtle, E.P.
1131 (2019). Titan seismology with Dragonfly: probing the internal structure of the most
1132 accessible ocean world. In: 50th Lunar and Planetary Science Conference. 2173.
- 1133 - Loveday, J. S., Nelmes, R. J., Guthrie, M., Belmonte, S. A., Allan, D. R., Klug, D. D.,
1134 Tse, J. S., & Handa, Y. P. (2001). Stable methane hydrate above 2 GPa and the
1135 source of Titan's atmospheric methane. *Nature*, 410, 661--663.
1136 <https://doi.org/10.1038/35070513>.
- 1137 - Luan, J. (2019). Titan's Dynamic Love Number Implies Stably-Stratified Ocean. *arXiv*
1138 [preprint arXiv:1905.03802](https://arxiv.org/abs/1905.03802).
- 1139 - Lunine, J. I., & Stevenson, D. J. (1987). Clathrate and ammonia hydrates at high
1140 pressure: Application to the origin of methane on Titan. *Icarus*, 70(1), 61--77.
1141 [https://doi.org/10.1016/0019-1035\(87\)90075-3](https://doi.org/10.1016/0019-1035(87)90075-3).

- 1142 - Marounina, N., Grasset, O., Tobie, G., & Carpy, S. (2018). Role of the global water
1143 ocean on the evolution of Titan's primitive atmosphere. *Icarus*, 310, 127--139,
1144 <http://doi.org/10.1016/j.icarus.2017.10.048>.
- 1145 - Meriggiola, R., & Iess, L. (2012). A new rotational model of Titan from Cassini SAR
1146 data. EPSC Abstracts, 7, EPSC2012-593, European Planetary Science Congress
1147 2012.
- 1148 - Miller, K. E., Glein, C. R., & Waite, J. H. Jr. (2019). Contributions from accreted
1149 organics to Titan's atmosphere: New insights from cometary and chondritic data.
1150 *Astrophys. J.*, 871, 59. <https://doi.org/10.3847/1538-4357/aaf561>.
- 1151 - Mitchell, J. L., & Lora, J. M. (2016). The climate of Titan. *Annu. Rev. Earth Planet. Sci.*,
1152 44(1), 353--380. <https://doi.org/10.1146/annurev-earth-060115-012428>.
- 1153 - Mitri, G., Showman, A. P., Lunine, J. I., & Lopes, R. M. C. (2008). Resurfacing of Titan
1154 by ammonia-water cryomagma. *Icarus*, 196(1), 216--224.
1155 <http://doi.org/10.1016/j.icarus.2008.02.024>.
- 1156 - Mitri, G., Meriggiola, R., Hayes, A., Lefevre, A., Tobie, G., Genova, A., Lunine, J. I., &
1157 Zebker, H. (2014). Shape, topography, gravity anomalies and tidal deformation of
1158 Titan. *Icarus*, 236, 169--177. <https://doi.org/10.1016/j.icarus.2014.03.018>.
- 1159 - Monteux, J., Coltice, N., Dubuffet, F., & Ricard, Y. (2007). Thermo-mechanical
1160 adjustment after impacts during planetary growth. *Geophys. Res. Lett.*, 34(24),
1161 L24201, <http://doi.org/10.1029/2007GL031635>.
- 1162 - Monteux, J., Tobie, G., Choblet, G., & Le Feuvre, M. (2014). Can large icy moons
1163 accrete undifferentiated?. *Icarus*, 237, 377--387.
1164 <http://doi.org/10.1016/j.icarus.2014.04.041>.
- 1165 - Mueller, S., & McKinnon, W. B. (1988), 3-layered models of Ganymede and Callisto -
1166 Compositions, structures, and aspects of evolution. *Icarus*, 76(3), 437--464.
1167 [http://doi.org/10.1016/0019-1035\(88\)90014-0](http://doi.org/10.1016/0019-1035(88)90014-0).
- 1168 - Murshed, M. M., Schmidt, B. C., & Kuhs, W. F. (2010). Kinetics of methane-ethane
1169 gas replacement in clathrate-hydrates studied by time-resolved neutron diffraction and
1170 Raman spectroscopy. *J. Phys. Chem. A*, 114, 247--255,
1171 <https://doi.org/10.1021/jp908016j>.
- 1172 - Nagel, K., Breuer, D., & Spohn, T. (2004). A model for the interior structure, evolution,
1173 and differentiation of Callisto. *Icarus*, 169(2), 402--412.
1174 <http://doi.org/10.1016/j.icarus.2003.12.019>.
- 1175 - Neish, C. D., & Lorenz, R. D. (2012). Titan's global crater population: A new
1176 assessment. *Planet. Space Sci.*, 60, 26--33, <http://doi.org/10.1016/j.pss.2011.02.016>.
- 1177 - Néri, A., Guyot, F., Reynard, B., & Sotin, C. (2020). A carbonaceous chondrite and
1178 cometary origin for icy moons of Jupiter and Saturn. *Earth Planet. Sci. Lett.*, 530(115),
1179 920. <https://doi.org/10.1016/j.epsl.2019.115920>.
- 1180 - Niemann, H. B., Atreya, S. K., Demick, J. E., Gautier, D., Haberman, J. A., Harpold,
1181 D. N., Kasprzak, W. T., Lunine, J. I., Owen, T. C., & Raulin, F. (2010). Composition of
1182 Titan's lower atmosphere and simple surface volatiles as measured by the Cassini-
1183 Huygens probe gas chromatograph mass spectrometer experiment. *J. Geophys. Res.*,
1184 115, E12006. <https://doi.org/10.1029/2010JE003659>.
- 1185 - Nimmo, F., & Bills, B. G. (2010). Shell thickness variations and the long-wavelength
1186 topography of Titan. *Icarus*, 208(2), 896--904.
1187 <http://doi.org/10.1016/j.icarus.2010.02.020>.

- 1188 - O'Rourke, J. G., & Stevenson, D. J. (2014). Stability of ice/rock mixtures with
1189 application to a partially differentiated Titan. *Icarus*, 227, 67--77.
1190 <http://doi.org/10.1016/j.icarus.2013.09.010>.
- 1191 - Requier, J., Trinh, A., Triana, S. A., & Dehant, V. (2019). Internal Energy Dissipation in
1192 Enceladus's Subsurface Ocean From Tides and Libration and the Role of Inertial
1193 Waves. *J. Geophys. Res. Planets*, 124(8), 2198--2212.
1194 <http://doi.org/10.1029/2019JE005988>.
- 1195 - Rovira-Navarro, M., Rieutord, M., Gerkema, T., Maas, L. R. M., van der Wal, W., &
1196 Vermeersen, B. (2019). Do tidally-generated inertial waves heat the subsurface
1197 oceans of Europa and Enceladus? *Icarus*, 321, 126--140.
1198 <http://doi.org/10.1016/j.icarus.2018.11.010>.
- 1199 - Sagan, C., & Dermott, S. F. (1982). The tide in the seas of Titan. *Nature*, 300(5894),
1200 731--733. <http://doi.org/10.1038/300731a0>.
- 1201 - Sasaki, T., Stewart, G. R., & Ida, S. (2010). Origin of the different architectures of the
1202 Jovian and Saturnian satellite systems. *Astrophys. J.*, 714(2), 1052--1064,
1203 <http://doi.org/10.1088/0004-637X/714/2/1052>.
- 1204 - Saur, J., Neubauer, F. M., & Glassmeier, K. H. (2010). Induced magnetic fields in
1205 solar system bodies. *Space science reviews*, 152(1-4), 391-421.
- 1206 - Sears, W. D. (1995). Tidal dissipation in oceans on Titan. *Icarus*, 113(1), 39--56.
1207 <http://doi.org/10.1006/icar.1995.1004>.
- 1208 - Senshu, H., Kuramoto, K., & Matsui, T. (2002). Thermal evolution of a growing Mars.
1209 *J. Geophys. Res. Planets*, 107(E12), 5118, <http://doi.org/10.1029/2001JE001819>.
- 1210 - Showman, A. P., & Malhotra, R. (1999). The Galilean satellites. *Science*, 286(5437),
1211 77--84. <http://doi.org/10.1126/science.286.5437.77>.
- 1212 - Simoes, F., Grard, R., Hamelin, M., Lopez-Morenoc, J. J., Schwingenschuh, K.,
1213 Beghin, C., Berthelier, J. J., Besser, B., Brown, V. J. G., Chabassiere, M., Falkner, P.,
1214 Ferri, F., Fulchignoni, M., Hofe, R., Jernej, I., Jeronimo, J. M., Molina-Cuberos, G. J.,
1215 Rodrigo, R., Svedhem, H., Tokano, T., Trautner, R. (2007). A new numerical model
1216 for the simulation of ELF wave propagation and the computation of eigenmodes in the
1217 atmosphere of Titan: Did Huygens observe any Schumann resonance? *Planet. Space*
1218 *Sci.*, 55(13), 1978--1989. <http://doi.org/10.1016/j.pss.2007.04.016>.
- 1219 - Sloan, E., Koh, C., & Koh, C. (2007). Clathrate hydrates of natural gases. *Chemical*
1220 *Industries*, CRC Press.
- 1221 - Soderlund, K. M. (2019). Ocean dynamics of outer solar system satellites. *Geophys.*
1222 *Res. Lett.*, 46(15), 8700-8710. <https://doi.org/10.1029/2018GL081880>.
- 1223 - Soderlund, K. M., Kalousová, K., Buffo, J. J., Glein, C. R., Goodman, J. C., Mitri, G.,
1224 Patterson, G. W., Postberg, F., Rovira-Navarro, M., Ruckriemen, T., Saur, J., Schmidt,
1225 B. E., Sotin, C., Spohn, T., Tobie, G., Van Hoolst, T., Vance, S. D., & Vermeersen, L.
1226 L. A. (2020). Ice-ocean exchange processes in the Jovian and Saturnian Satellites.
1227 *Space Sci. Rev.*, 216(80). <http://doi.org/10.1007/s11214-020-00706-6>.
- 1228 - Sohl, F., Sears, W. D., & Lorenz, R. D. (1995). Tidal dissipation on Titan. *Icarus*,
1229 115(2), 278--294. <http://doi.org/10.1006/icar.1995.1097>.
- 1230 - Sohl, F., Spohn, T., Breuer, D., & Nagel, K. (2002). Implications from Galileo
1231 observations on the interior structure and chemistry of the Galilean satellites. *Icarus*,
1232 157(1), 104--119, <http://doi.org/10.1006/icar.2002.6828>.
- 1233 - Sotin, C., & Poirier, J.-P. (1987). Viscosity of ice V. *J. Phys., Colloq.*, 48 (C1), 233--
1234 238. <https://doi.org/10.1051/jphyscol:1987132>.

- 1235 - Sotin, C., Gillet, P., & Poirier, J.-P. (1985). Creep of high-pressure ice VI. In: Klinger,
1236 J., Benest, D., Dollfus, A., Smoluchowski, R. (Eds.), *Ices in the Solar System*. Reidel,
1237 Dordrecht, Netherlands, pp.109–118.
- 1238 - Stiles, B. W., Kirk, R. L., Lorenz, R. D., Hensley, S., Lee, E., Ostro, S. J., Allison, M.
1239 D., Callahan, P. S., Gim, Y., Iess, L., del Marmo, P. P., Hamilton, G., Johnson, W. T.
1240 K., West, R. D., and The Cassini RADAR Team (2008), Determining Titan's spin state
1241 from Cassini radar images. *Astron. J.*, 135(5), 1669--1680.
1242 <https://doi.org/10.1088/0004-6256/135/5/1669>.
- 1243 - Stiles, B. W., Kirk, R. L., Lorenz, R. D., Hensley, S., Lee, E., Ostro, S. J., Allison, M.
1244 D., Callahan, P. S., Gim, Y., Iess, L., del Marmo, P. P., Hamilton, G., Johnson, W. T.
1245 K., West, R. D., and The Cassini RADAR Team (2010). Erratum: "Determining Titan's
1246 spin state from Cassini radar images" (2008, *AJ*, 135, 1669). *Astron. J.*, 139(1), 311--
1247 311, <http://doi.org/10.1088/0004-6256/139/1/311>.
- 1248 - Stofan, E. R., Elachi, C., Lunine, J. I., Lorenz, R. D., Stiles, B., Mitchell, K. L., Ostro,
1249 S., Soderblom, L., Wood, C., Zebker, H., Wall, S., Janssen, M., Kirk, R., Lopes, R.,
1250 Paganelli, F., Radebaugh, J., Wye, L., Anderson, Y., Allison, M., Boehmer, R.,
1251 Callahan, P., Encrenaz, P., Flamini, E., Francescetti, G., Gim, Y., Hamilton, G.,
1252 Hensley, S., Johnson, W. T. K., Kelleher, K., Muhleman, D., Paillou, P., Picardi, G.,
1253 Posa, F., Roth, L., Seu, R., Shaffer, S., Vetrella, S., & West, R. (2007). The lakes of
1254 Titan. *Nature*, 445, 61–64. <https://doi.org/10.1038/nature05438>.
- 1255 - Tobie, G., Grasset, O., Lunine, J. I., Mocquet, A., & Sotin, C. (2005a). Titan's internal
1256 structure inferred from a coupled thermal-orbital model. *Icarus*, 175(2), 496–502.
1257 <https://doi.org/10.1016/j.icarus.2004.12.007>.
- 1258 - Tobie, G., Mocquet, A., & Sotin, C. (2005b). Tidal dissipation within large icy satellites:
1259 Applications to Europa and Titan. *Icarus*, 177(2), 534–549.
1260 <https://doi.org/10.1016/j.icarus.2005.04.006>.
- 1261 - Tobie, G., Lunine, J. I., & Sotin, C. (2006). Episodic outgassing as the origin of
1262 atmospheric methane on Titan. *Nature*, 440, 61–64.
1263 <https://doi.org/10.1038/nature04497>.
- 1264 - Tobie, G., Choukroun, M., Grasset, O., Le Mouelic, S., Lunine, J. I., Sotin, C.,
1265 Bourgeois, O., Gautier, D., Hirtzig, M., Lebonnois, S., & Le Corre, L. (2009). Evolution
1266 of Titan and implications for its hydrocarbon cycle. *Philos. Trans. R. Soc. A*, 367(1889),
1267 617-631. <http://doi.org/10.1098/rsta.2008.0246>.
- 1268 - Tobie, G., Gautier, D., & Hersant, F. (2012). Titan's Bulk Composition Constrained by
1269 Cassini-Huygens: Implication for Internal Outgassing. *Astrophys. J.*, 752(2), 125,
1270 <http://doi.org/10.1088/0004-637X/752/2/125>.
- 1271 - Tobie, G., Lunine, J., Monteux, J., Mousis, O., & Nimmo, F. (2014). The origin and
1272 evolution of Titan. In I. Müller-Wodarg, C. Griffith, E. Lellouch, & T. Cravens (Eds.),
1273 *Titan: Interior, Surface, Atmosphere, and Space Environment* (Cambridge Planetary
1274 Science, pp. 29-62). Cambridge: Cambridge University Press.
1275 <http://doi.org/10.1017/CBO9780511667398.004>.
- 1276 - Turtle, E. P., Barnes, J. W., Trainer, M. G., Lorenz, R. D., MacKenzie, S. M., Hibbard,
1277 K. E., Adams, D., Bedini, P., Langelaan, J. W., Zacny, K., & the Dragonfly Team
1278 (2017). Dragonfly: Exploring Titan's prebiotic organic chemistry and habitability, in
1279 lunar and planetary science conference. *Lunar and Planetary Science Conference*,
1280 48, 1958.
- 1281 - Tyler, R. H. (2008). Strong ocean tidal flow and heating on moons of the outer planets.
1282 *Nature*, 456(7223), 770--772. <http://doi.org/10.1038/nature07571>.

- 1283 - Vance, S., Bouffard, M., Choukroun, M., & Sotin, C. (2014). Ganymede's internal struc-
1284 ture including thermodynamics of magnesium sulfate oceans in contact with ice.
1285 Planet. Space Sci., 96, 62–70. <https://doi.org/10.1016/j.pss.2014.03.011>.
- 1286 - Vance, S. D., & Brown, J. M. (2013). Thermodynamic properties of aqueous MgSO₄
1287 to 800 MPa at temperatures from -20 to 100°C and concentrations to 2.5 mol kg⁻¹ from
1288 sound speeds, with applications to icy world oceans. Geochim. Cosmochim. Acta, 110,
1289 176–189, <http://doi.org/10.1016/j.gca.2013.01.040>.
- 1290 - Vance, S. D., Panning, M. P., Stahler, S., Cammarano, F., Bills, B. G., Tobie, G.,
1291 Kamata, S., Kedar, S., Sotin, C., Pike, W. T., Lorenz, R., Huang, H. H., Jackson, J.
1292 M., & Banerdt, B. (2018). Geophysical investigations of habitability in ice-covered
1293 ocean worlds. J. Geophys. Res. Planets, 123(1), 180–205.
1294 <http://doi.org/10.1002/2017JE005341>.
- 1295 - Van Hoolst, T., Rambaux, N., Karatekin, O., & Baland, R.-M. (2009). The effect of
1296 gravitational and pressure torques on Titan's length-of-day variations. Icarus, 200(1),
1297 256–264. <http://doi.org/10.1016/j.icarus.2008.11.009>.
- 1298 - Van Hoolst, T., Baland, R.-M., & Trinh, A. (2013), On the librations and tides of large
1299 icy satellites. Icarus, 226(1), 299–315. <http://doi.org/10.1016/j.icarus.2013.05.036>.
- 1300 - Vu, T. H., Choukroun, M., Sotin, C., Muñoz-Iglesias, V., & Maynard-Casely, H. E.
1301 (2020). Rapid formation of clathrate hydrate from liquidthane and water ice on Titan.
1302 Geophys. Res. Lett., 47, e2019GL086265. <https://doi.org/10.1029/2019GL086265>.
- 1303 - Wagner, W., Saul, A., & Pruss, A. (1994). International equations for the pressure
1304 along the melting and along the sublimation curve of ordinary water substance. J.
1305 Phys. Chem. Ref. Data, 23(3), 515–527. <https://doi.org/10.1063/1.555947>.
- 1306 - Wagner, W., Riethmann, T., Feistel, R., & Harvey, A.H. (2011). New equations for the
1307 sublimation pressure and melting pressure of H₂O ice Ih. J. Phys. Chem. Ref. Data,
1308 40(4), 043103. <https://doi.org/10.1063/1.3657937>.
- 1309 - Wasson, J. T., & Kallemeyn, G. W. (1988). Composition of chondrites. Philos. Trans.
1310 R. Soc. Lond. Ser. A, Math. Phys. Sci., 325(1587), 535–544.
1311 <http://doi.org/10.1098/rsta.1988.0066>.
- 1312 - Werynski, A., Neish, C., Gall, A. L., & Janssen, M. (2019). Compositional variations of
1313 Titan's impact craters indicates active surface erosion. Icarus, 321, 508–521.
1314 <https://doi.org/10.1016/j.icarus.2018.12.007>.
- 1315 - Yung, Y. L., Allen, M., & Pinto, J. P. (1984). Photochemistry of the atmosphere of Titan:
1316 Comparison between model and observations. Astrophys. J. Suppl. Ser., 55, 465–
1317 506. <https://doi.org/10.1086/190963>.
- 1318 - Zahnle, K. J., Korycansky, D. G., & Nixon, C. A. (2014). Transient climate effects of
1319 large impacts on Titan. Icarus, 229, 378–391.
- 1320 - Zebker, H. A., Gim, Y., Callahan, P., Hensley, S., Lorenz, R., & the Cassini Radar
1321 Team (2009). Analysis and interpretation of Cassini Titan radar altimeter echoes.
1322 Icarus, 200(1), 240–255. <http://doi.org/10.1016/j.icarus.2008.10.023>.
- 1323